

Geochemical and isotopic (Nd and Sr) constraints on elucidating the origin of intrusions from northwest Saveh, Central Iran

Mehdi Rezaei-Kahkhaei^{1*}, Dariush Esmaily², Carmen Galindo Francisco³

¹ Department of Petrology and Economic Geology, Faculty of Earth Sciences, Shahrood University, Iran

² Department of Geology, University College of Sciences, University of Tehran, Tehran, Iran

³ Departamento de Petrología y Geoquímica. Universidad Complutense –IGE (CSIC). C/ José Antonio Novais, n 2, 28040-Madrid, Spain

*Corresponding author, e-mail: Rezaei@Shahroodut.ac.ir

(received: 15/10/2013 ; accepted: 06/07/2014)

Abstract

Three intrusive granitoid bodies from northwest Saveh, central Iran, are embedded in volcanic sedimentary rocks of the Eocene, forming isolated small outcrops: Khalkhab quartz monzodioritic units (SiO₂: ~52-57 wt %) to the northwest, Neshveh granodioritic units (SiO₂: ~62-71 wt %) to the northeast, and Selijerd granodioritic units (SiO₂: ~63-69 wt %) to the southeast. The Khalkhab unit is composed of quartz monzogabbro and quartz monzodiorite with medium- to coarse-grained textures. The Neshveh unit is composed mainly of granodiorite with subordinate granite of medium grain size and a porphyritic texture with plagioclase megacryst. The Selijerd unit ranges from granodiorite to tonalite with a medium- to coarse-grained granophyric texture. The rocks studied display a relatively high Na₂O content, with a molecular A/CNK ratio less than 1.1, Na₂O/ K₂O ratio of ~2.06 and calc-alkaline affinity. They contain modal clinopyroxene, hornblende, magnetite and titanite, suggesting I-type characteristics for these rocks and formation in an active continental margin. Isotopic data (⁸⁷Sr/⁸⁶Sr_{39Ma} = 0.704536-0.704860; ε(Nd)_{39Ma} = 2.2-3.9) from northwest Saveh intrusive rocks are plotted to the left of bulk silicate Earth. These ratios, together with geochemical data, suggest that the parent magmas of the rocks studied might be generated by crystal fractionation of arc basalts in crustal magma chambers, coupled with some lower crustal assimilation prior to silica enrichment, to form quartz monzogabbros. Consequently, granodiorites formed dominantly by crystal fractionation from evolved parental magmas that ascended into the upper crustal magma chambers.

Keywords: Saveh; Fractional Crystallization; I-Type Granitoid; Volcanic Arc; Central Iran.

Introduction

The tectonic history of the Neotethys region has been studied by many authors (e.g., Ricou, 1971; Berberian & Berberian, 1981; Berberian *et al.*, 1982; Molinaro *et al.*, 2005; Ghasemi & Talbot, 2006, among others). The protracted convergence history between Afro-Arabia and Eurasia (150 Ma to present), comprising a long-lasting period of subduction, started from the late Triassic to early Jurassic (Berberian & Berberian, 1981; Arvin *et al.*, 2007) and was followed by collision during the Tertiary (Omran *et al.*, 2008). Prior to collision, major geological and kinematic changes had also taken place in the Neotethys (Ricou, 1994; Agard *et al.*, 2007) that triggered regional-scale thrusting of oceanic lithosphere at ~95 Ma and ophiolite emplacement onto Arabia during the late Cretaceous (Ricou, 1971; Boudier *et al.*, 1988; Nicolas, 1989; Searle & Cox, 1999; Ghasemi & Talbot, 2006).

The Zagros orogenic belt of Iran, which is a part of the Alpine-Himalayan orogenic belt, consists of three parallel tectonic subdivisions from southeast to northwest (Alavi, 1994). These are (1) the

Zagros fold-and-thrust belt (2) the Sanandaj-Sirjan magmatic arc (SSMA) and (3) the Urumieh-Dokhtar magmatic arc (UDMA, Fig. 1). Collision in the Zagros has been studied recently in terms of geophysics, kinematics and neotectonics (McQuarrie *et al.*, 2003; Talebian & Jackson, 2004; Vernant *et al.*, 2004; Molinaro *et al.*, 2004; 2005; Meyer *et al.*, 2005; Agard *et al.*, 2006, 2007). Little is known, however, about the long-lasting magmatic activity (~150 Ma) of the two presumably subduction-related arcs trending parallel to the Main Zagros Thrust, the Mesozoic SSMA and the Tertiary to Plio-Quaternary UDMA. Compared to a few studies on the SSMA (Berberian & Berberian, 1981; Berberian *et al.*, 1982; Ahmadi Khalaji *et al.*, 2007), the internal UDMA remains poorly studied, despite being one of the best preserved active margins within the greater Alpine-Himalayan convergence system.

Arc magmatism provides useful information about mantle geochemical evolution and crust-melting processes in subduction zones (e.g., Pearce *et al.*, 1990; Davidson, 1996; Macdonald *et al.*, 2000). In the case of UDMA, it should also help us

to solve some first-order geodynamic problems. For instance, how an area of about 300 km far from the proposed subduction front could be the result of subduction of Neothethyan oceanic lithosphere beneath the central Iran continental lithosphere.

In this paper, we integrate field observations, petrographic studies, and whole-rock geochemistry including Sr–Nd isotopes to elucidate the petrogenesis of intrusions from northwest Saveh.

On the basis of these data, we infer a petrologic model that explains the systematic variation in the composition of the three intrusions. These observations provide information towards a better understanding of the tectonic evolution of the UDMA, which is one of the more poorly understood zones of the central Iranian terrain and related magmatism in Iran.

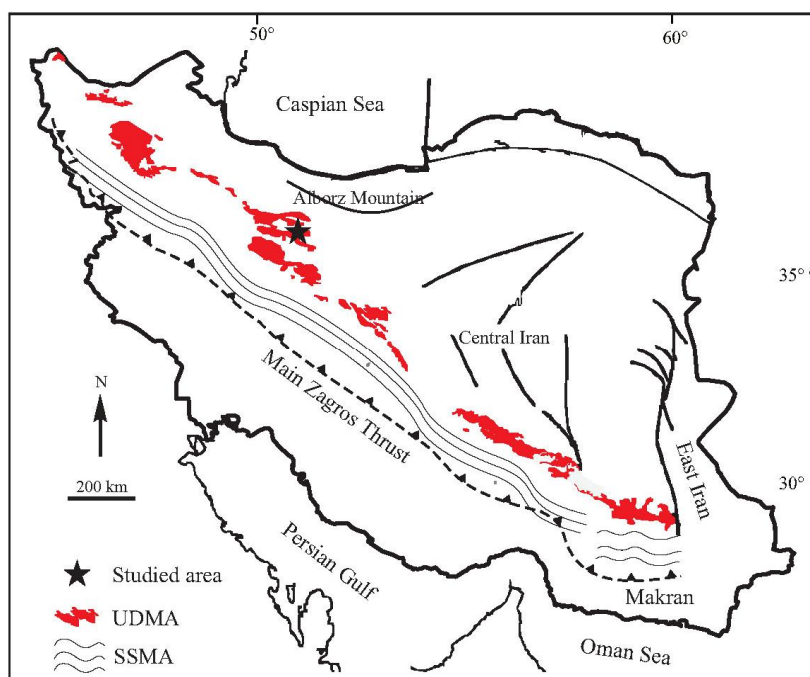


Figure 1: Two presumably subduction-related arcs trending parallel to the Main Zagros Thrust are shown on the simplified map of Iran. The Mesozoic Sanandaj-Sirjan magmatic arc (SSMA); the Tertiary to Plio-Quaternary Urumieh Dokhtar magmatic arc (UDMA). The location of northwest Saveh intrusions is shown by a star.

Geological setting

The northwest Saveh intrusions, covering an area of ~124 km² (Fig. 2), are an array of plutonic massifs within the 1800 km-long, NW-SE trending UDMA (Fig. 1). The UDMA, running from eastern Turkey to southeast Iran, is mainly composed of Eocene-Miocene volcano-sedimentary sequences and associated plutonic rocks (Berberian & Berberian, 1981; Berberian *et al.*, 1982; Mobasher & Babaie, 2008). It represents an important metalliferous region due to the presence of Cu-Fe-Au-Mo-W deposits. Magmatism occurred principally during the Eocene but has later been reactivated, after a quiescent period, during the Upper Miocene to Plio-Quaternary. Although most of the igneous rocks of the UDMA are calc-alkaline, some volcanic rocks show alkaline or shoshonitic affinity (Arvin *et al.*, 2007; Omrani *et al.*, 2008).

Previous studies of the northwest Saveh intrusions were mostly limited to reconnaissance reports and maps of various scales (Amidi, 1984; Ghalamghash, 1998). The study area is bounded by the Koushk-Nousrat and Neshveh faults in the north and the Saveh fault in the south (Fig. 2).

The country rocks of the northwest Saveh intrusions are volcano-sedimentary (Figs. 3a, b). Their contacts are commonly irregular (Fig. 3a) and occasionally faulted (Figs. 3c, d). Some of the volcanic rocks experienced low-grade metamorphism, especially near the irregular contacts, and their minerals (e.g., plagioclase and pyroxene) were altered to calcite and chlorite.

Volcanic rocks are dominated by successions of andesitic lava and rhyo-dacitic tuff, andesitic-basaltic lava and andesitic-basaltic breccias, locally associated with limestone (Ghalamghash, 1998;

Davarpanah, 2009). The andesitic lava and rhyodacitic tuff, which are the oldest rocks, are exposed in the central part of the mapped area and are the main wall rocks of the studied plutonic rocks (Fig. 2). The rhyo-dacitic tuff is mainly made of volcanic fragments, mostly ejected glass shards due to explosive acidic eruptions in the marine environment (now devitrified) and other fragments, forming green minerals such as chlorite and epidote, with various clay minerals (Winter, 2001). Andesitic and basaltic lavas outcrop in a scattered way in the mapped area (Fig. 2), which are dark green and brown in colour and have minor beds of

andesitic tuff. They are mainly composed of plagioclase, olivine and pyroxene. The andesitic-basaltic breccias are exposed in the northwest of the area (Fig. 2). They are made of a sequence of hyaloclastic breccias and tuff at the base, which grade upward into massive plagioclase phyric lava. They are also followed by aphyric lava and autoclastic breccias at the top (Davarpanah, 2009). A recent petrological and geochemical study of the volcanic rocks suggests that these are formed in a subduction setting and are derived from a mantle lithospheric source (Davarpanah, 2009).

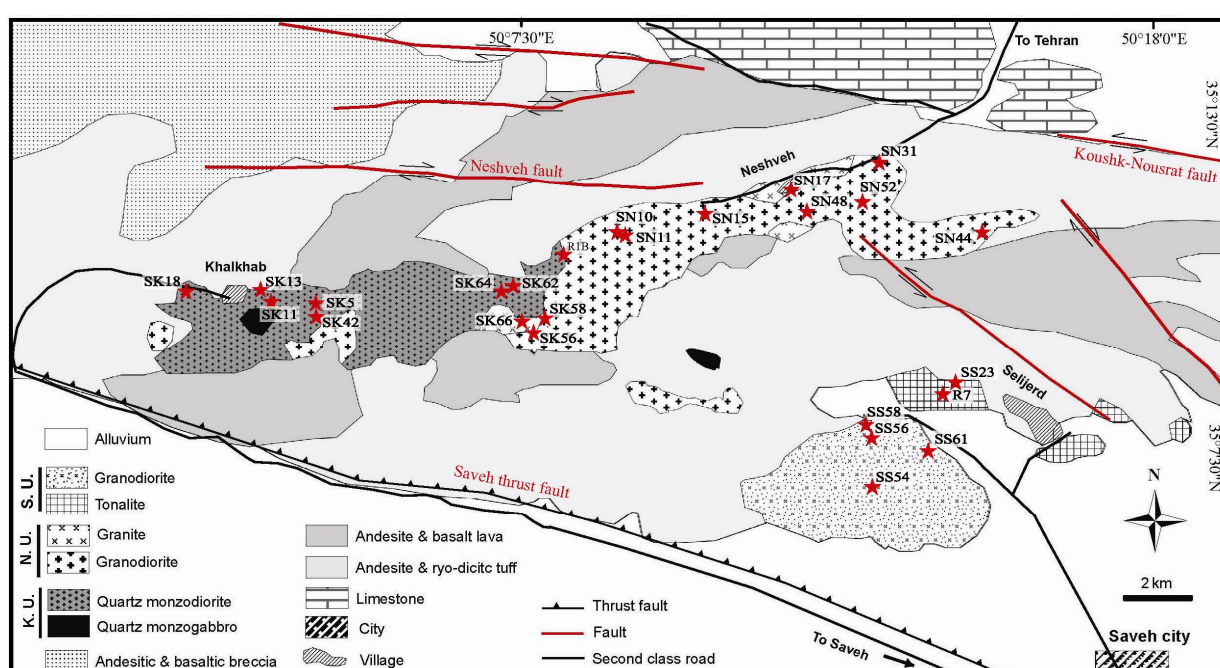


Figure 2: Simplified geological map of northwest Saveh intrusions (based on satellite data and the geological map of Saveh 1: 100,000; Ghalamghash 1998). Abbreviations: K.U. Khalkhab unit; N.U. Neshveh unit; S.U. Selijerd unit.

The volcanic rocks are covered with thin to medium sized limestone beds (Fig. 3b). Moreover, a sequence of sedimentary rocks is observed in the northern part of the mapped area, forming medium to thick beds of sandy-gravelly limestone and marl. We have found the following microfossils in this sequence: *Elphidium* sp. 14, *Archaias kirkukensis*, *Archaias asmaricus*, *Astrigrina rotula*, *Rotalia* sp., *Borelis* sp., *Austrotrilina*, *Miogypsinoides*, *Lepidocylicina* with Aquitanian age (23.0–20.4 Ma). It thus seems that the northwest Saveh intrusions must be older than Aquitanian.

Petrography and field relationship

Detailed mapping of the northwest Saveh intrusions reveals three main units (Ghalamghash, 1998),

hereafter referred to Khalkhab quartz monzodiorite unit, Neshveh granodiorite unit and Selijerd granodiorite unit (Fig. 2).

Khalkhab quartz monzodiorite unit

The Khalkhab quartz monzodiorite unit covers an area of ~27 km² (9 km long and 3 km wide), and crops out in the northwestern part of the area (Fig. 2). Rocks are generally medium- to coarse-grained with granular to intergranular texture (Fig. 4a). They are either quartz monzogabbro or quartz monzodiorite, mainly composed of plagioclase (51–56 modal%) + K-feldspar (9–14 modal%) + quartz (8–12 modal%) ± clinopyroxene (5–26 modal%) ± hornblende (7–14 modal%) (Figs. 4a, b). Apatite and opaque minerals are the main accessory

minerals. Subhedral clinopyroxenes are replaced by actinolite and biotite aggregates in some samples. Green hornblende occurs as a subhedral to euhedral mineral, sometimes accompanied by biotite. Plagioclase forms mainly euhedral to subhedral lath-shape crystals. It mainly shows zoning,

twinning and prismatic-cellular growth. Sometimes plagioclase is altered to sericite and clay minerals. K-feldspar and quartz occur as anhedral and interstitial minerals in the quartz monzogabbros. They occasionally show a graphic intergrowth.

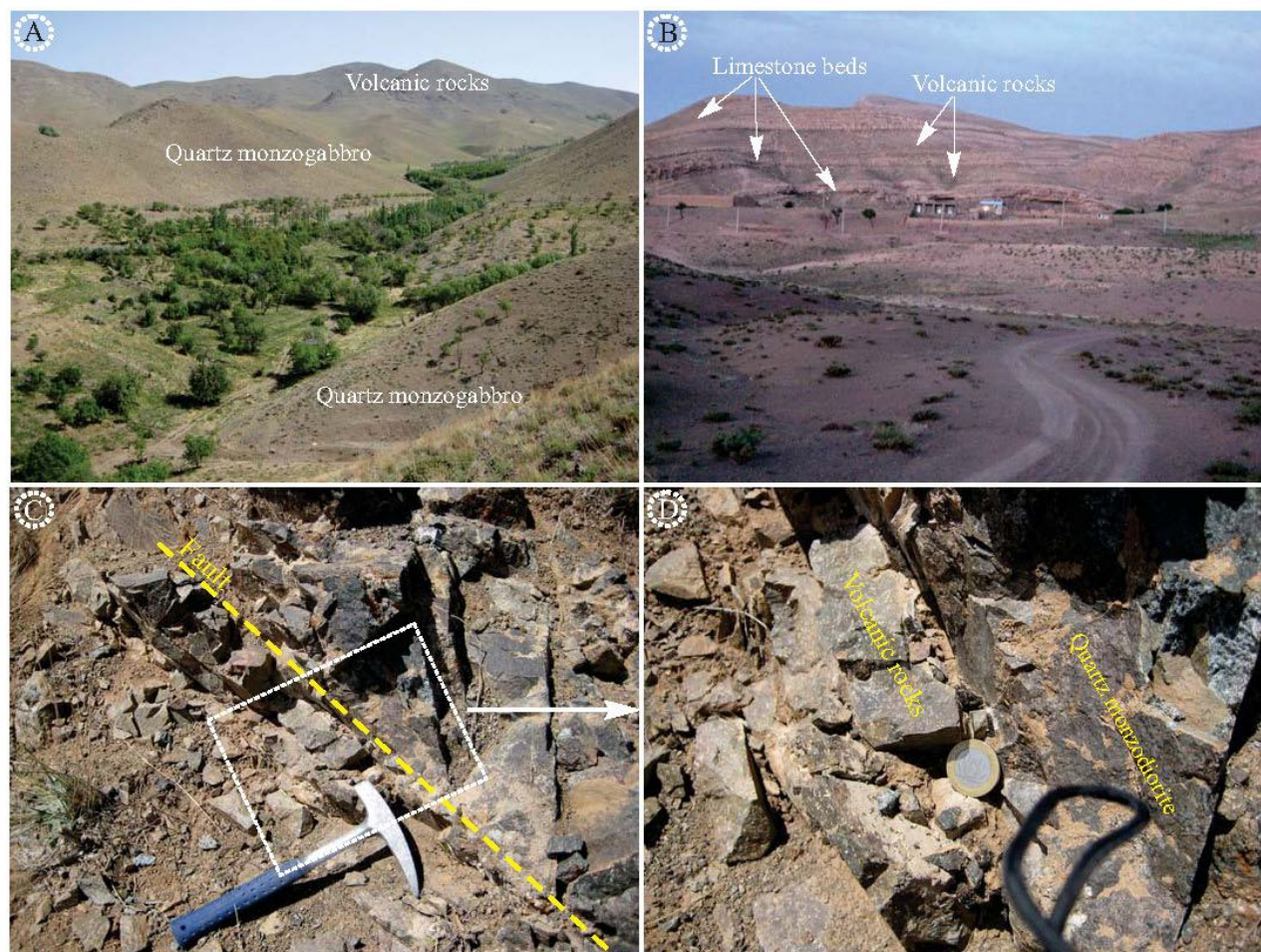


Figure 3: A. Northwest Saveh intrusive rocks emplaced into the volcanic rocks. B. The volcanic rocks intersecting thin to medium limestone beds. C and D show a faulted contact between quartz monzogabbro and volcanic rocks.

Neshveh granodiorite unit

The eastern and central parts of the area are mainly composed of granodiorite with subordinate granite. They have generally transitional contact with the Khalkhab quartz monzodiorite unit. The granodioritic rocks are generally medium- to coarse-grained with a white to pink colour. The mineral assemblage includes plagioclase (41-44 modal%), K-feldspar (15-19 modal%), quartz (17-20 modal%), hornblende (11-13 modal%), biotite (3-5 modal%), Fe-Ti oxides (2-3 modal%) and clinopyroxene (<3 modal%) (Fig. 4c). Titanite, zircon and apatite are rare. The main mafic phases are idiomorphic hornblende and biotite. Sometimes

rare clinopyroxene rimmed by hornblende, biotite, and Fe-Ti oxides appears. Plagioclase occurs as zoned subhedral crystals, usually twinned, of 0.3-1 mm in size. Subhedral or anhedral K-feldspar crystals are particularly altered to clay minerals in some thin sections. Green hornblende is euhedral to subhedral and sometimes appears spatially related to biotite.

The granites mostly appear in the central part of the Neshveh unit. They are generally medium-grained and have granular to porphyritic texture with megacrysts of plagioclase (Fig. 4d). They contain plagioclase (32-41.1 modal%), K-feldspar (25-29.7 modal%) and quartz (65.1-69.4 modal%),

with mafic minerals such as green hornblende (2.3–11.2 modal%) and biotite (<2.2 modal%). Plagioclase is normally zoned and sometimes altered to sericite. Green hornblende is partially

replaced by chlorite and opaque minerals in few samples. Opaque minerals are magnetite and hematite.

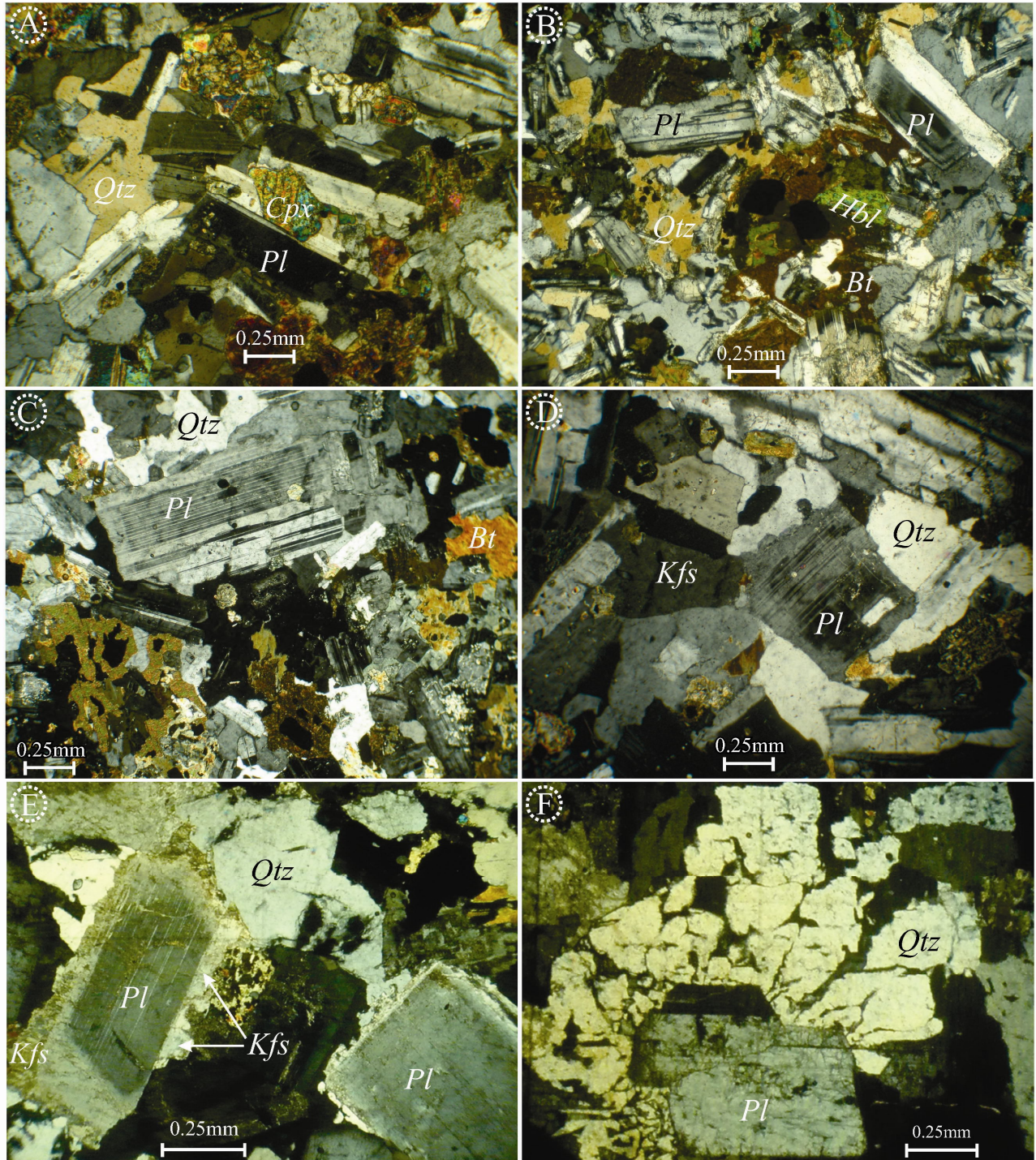


Figure 4: A. Quartz monzogabbro with granular texture and B. Quartz monzodiorite, composed mainly of plagioclase, hornblende and quartz from the Khalkhab unit. C. Granodiorite with megacryst of quartz and D. granite from the Neshveh unit. E. Plagioclase displays an anti-rapakivi texture and F. Granophyric-like texture around plagioclase (globular intergrowth) from the Selijerd unit. Abbreviations: Qtz: quartz; Pl: plagioclase; Cpx: clinopyroxene; Hbl: hornblende; Bt: biotite; Kfs: K-feldspar (Kretz 1983).

Selijerd granodiorite unit

The Selijerd granodiorite unit comprises small isolated outcrops mostly outcropping in the southeastern part of the studied area (Fig. 2). The rocks range petrographically from tonalite with a medium-grained texture to granodiorite with a coarse-grained texture.

Tonalites mainly occur in the margin, mostly in the northern part of this plutonic ensemble (Fig. 2). They are grey to light grey in colour and mainly consist of plagioclase (~57-62 modal%), quartz (~21-27 modal%), green-to-brown hornblende (~10-15 modal%), K-feldspar (~4-7 modal%) and some opaque minerals. Accessory minerals comprise apatite, zircon and titanite. Plagioclase is subhedral to euhedral and locally rimmed (partly or completely) by K-feldspar, displaying local anti-rapakivi texture. Green-to-brown hornblendes are anhedral to subhedral and occasionally altered to actinolite and opaque minerals. K-feldspar occurs mostly as small to medium anhedral grains, and partially altered to clay minerals.

Granodiorites are medium- to coarse-grained and white in colour. They occur within the centre of the main Selijerd pluton, an elliptically shaped massive of 19 km² (Fig. 2). Plagioclases appear as euhedral to ovoid crystals and are often rimmed (partly or completely) by K-feldspar, displaying a local anti-rapakivi-texture (Fig. 4e). Plagioclase crystals are commonly zoned and sporadically altered to fine-grained sericite. Quartz and K-feldspar occasionally display graphic intergrowth (Fig. 4f), rimming same plagioclase crystals and giving rise to granophyric or micrographic-like texture (globular intergrowth). Quartz is anhedral with distinct undulose extinction. Quartz also appears interstitial in some samples.

Geochemistry

Sampling and analytical methods

A total of about 185 rock samples were collected from different localities, and then 150 thin sections were studied by optical microscope. Twenty-six representative samples were selected for whole rock chemical analyses and six of them for Sr and Nd isotopic analyses. Samples weighed between 1-1.5 kg before crushing and powdering. Major and trace element abundances were determined by inductively coupled plasma atomic emission spectrometry (ICP-AES) and inductively coupled plasma mass spectrometry (ICP-MS) at the ALS

Chemex laboratory in Vancouver, Canada. Detection limits range within 0.01-0.1 wt% for major oxides, 0.1-10 ppm for trace elements, and 0.01-0.5 ppm for the rare earth elements.

Concentrations of Rb and Sr as well as Rb/Sr atomic ratios were determined by X-ray fluorescence spectrometry at the X-Ray Diffraction Centre of the Complutense University (Madrid, Spain). Isotope ratio measurements were made on a VG Sector 54 mass spectrometer at the Geochronology and Isotope Geochemistry Centre of the Complutense University. Sm and Nd concentrations were determined by isotope dilution using a mixed ¹⁴⁹Sm-¹⁵⁰Nd spike solution. Sr and REE were separated using DOWEX 50W-X 12 200-400 mesh cation exchange resins. Sm and Nd were further separated from the REE group using cation-exchange columns filled with bio-beads coated with 10% HDEHP. Errors are quoted as two standard deviations from measured or calculated values. The decay constants used in the calculations are: $\lambda^{87}\text{Rb} = 1.42 \times 10^{-11}$ and $\lambda^{147}\text{Sm} = 6.54 \times 10^{-12} \text{ year}^{-1}$ recommended by the IUGS Subcommission for Geochronology (Steiger & Jaeger, 1977). Analytical uncertainties are estimated to be 0.01% for ⁸⁷Sr/⁸⁶Sr ratios and 0.006% for ¹⁴³Nd/¹⁴⁴Nd ratios and 1% and 0.1% for the ⁸⁷Rb/⁸⁶Sr and ¹⁴⁷Sm/¹⁴⁴Nd ratios respectively. Epsilon-Nd (ϵNd) values were calculated relative to a chondrite present-day ¹⁴³Nd/¹⁴⁴Nd value of 0.512638 and ¹⁴⁷Sm/¹⁴⁴Nd of 0.1967. Replicate analyses of NBS 987 yielded an average ⁸⁷Sr/⁸⁶Sr = 0.710203 ± 0.00004 (2 σ ; σn =10). Analyses of La Jolla yielded an average ¹⁴³Nd/¹⁴⁴Nd = 0.511844 ± 0.00002 (2 σ ; σn =7).

Major and trace elements

Major and trace element analyses for the northwest Saveh intrusions are presented in Table 1 and their variations versus SiO₂ are plotted in Harker diagrams (Figs. 5, 6). SiO₂ contents of different samples range from 52.1-56.7 wt% for the Khalkhab quartz-monzodiorite unit, 59.6-71.2 wt% for the Neshveh granodiorite unit and 63.3-68.9 wt% for the Selijerd granodiorite unit (Table 1).

As seen in Figs. 5 and 6, the Selijerd unit defines a distinct magmatic group, while the Khalkhab and Neshveh units show similar trends. The Khalkhab and Neshveh samples show negative correlation between TiO₂, Al₂O₃, MgO, CaO, MnO, P₂O₅, Fe₂O₃, Ni, Co and V with SiO₂; and positive

correlation between K₂O, Ba, Rb, Nb, La, Ce and Zr with SiO₂. The correlations of Na₂O and Sr are positive up to SiO₂ = 55 wt% and negative from

this point onward. Positive correlations are less defined than the negative ones (Figs. 5, 6).

Table 1: Whole-rock major (wt%) and trace (ppm) element compositions of the northwest Saveh intrusive samples. (Continued on the next page)

Intrusion Rock types	Khalkhab unit								
	Quartz monzogabbro					Quartz monzodiorite			
Sample no.	SK11	SK42	SK18	SK5	SK58	SK64	SN10	SK62	R1B
SiO ₂ [†]	52.1	52.2	53.2	54.7	55.1	55.5	56.5	56.7	57.56
TiO ₂ [†]	0.93	1.01	0.82	0.87	0.74	0.8	0.73	0.75	0.66
Al ₂ O ₃ [†]	17.05	14.9	16.25	17.85	17.95	16.45	17.1	16.55	16.84
Fe ₂ O ₃ [†]	11.1	12.85	10.3	8.96	8.95	8.59	8.66	9.38	
FeO [†]									7.21
MnO [†]	0.19	0.29	0.3	0.22	0.11	0.12	0.14	0.2	0.15
MgO [†]	4.08	4.11	4.43	2.32	3.1	3.75	3.26	3.6	2.73
CaO [†]	7.44	7.71	6.33	6.83	7.06	7.66	7.16	7.71	5.97
Na ₂ O [†]	3.39	2.42	3.1	4.09	3.68	3.82	3.23	3.14	3.46
K ₂ O [†]	1.48	1.88	2.1	1.62	1.93	1.21	1.85	1.76	2.08
P ₂ O ₅ [†]	0.23	0.26	0.15	0.43	0.26	0.25	0.23	0.22	0.2
Total	97.99	97.63	96.98	97.89	98.88	98.15	98.86	100.01	96.86
V [‡]	353	426	338	208	226	295	241	269	136
Cr [‡]	30	10	20	10	10	30	20	30	20
Ni [‡]	16	13	14	6	7	13	14	11	20
Co [‡]	30.3	32.4	29.8	15.8	18.5	17.7	23.8	24.4	16
Cu [‡]	264	121	451	36	49	33	53	52	10
Zn [‡]	104	120	169	66	45	49	51	92	41
Ga [‡]	17.9	16.9	17.3	18	18.1	17.1	17.5	16.7	17
Sn [‡]	1	1	1	1	1	1	2	1	9
W [‡]	1	1	1	1	1	1	1	2	1
Ba [‡]	341	422	554	361	495	247	465	428	582
Sr [‡]	391	336	369	403	589	347	503	383	379
Rb [‡]	33.1	38.6	46.1	40.4	40.4	27.9	48.7	43.3	43
Nb [‡]	4.4	5.5	4.3	6.1	4.3	4.9	4.8	4.6	6.6
Y [‡]	22.4	25.3	21.3	27.7	21.7	23.9	20.9	25	20.3
Zr [‡]	81	81	79	121	72	94	83	95	101
Cs [‡]	1.25	0.67	0.87	0.68	1.19	0.74	1.95	1.5	1.3
Hf [‡]	2.4	2.8	2.4	3.6	2.2	2.9	2.4	2.8	2.9
Ta [‡]	0.3	0.4	0.3	0.4	0.3	0.3	0.3	0.3	0.39
Th [‡]	3.35	5.69	3.39	5.41	2.72	4.02	3.17	3.56	3.75
U [‡]	0.99	1.38	1.02	1.64	0.73	1.15	0.71	1.02	0.9
La [‡]	10.9	12.9	9.6	14.1	13.7	11.5	14	11.8	14.9
Ce [‡]	22.3	26.4	20	28.5	28.2	23.7	28.4	24.5	30.3
Pr [‡]	2.97	3.57	2.62	3.73	3.7	3.07	3.64	3.22	3.57
Nd [‡]	12.9	14.5	11.2	15.9	15.4	13.3	14.9	13.5	14.7
Sm [‡]	3.18	3.68	2.85	3.91	3.64	3.24	3.38	3.31	3.64
Eu [‡]	0.97	1.06	0.93	1.2	1.02	0.95	0.99	1.05	1.08
Gd [‡]	3.96	4.21	3.42	4.62	3.92	3.83	3.67	4.24	3.61
Tb [‡]	0.61	0.72	0.57	0.75	0.62	0.64	0.59	0.69	0.66
Dy [‡]	4.02	4.62	3.83	4.85	3.92	4.12	3.73	4.38	3.85
Ho [‡]	0.83	0.94	0.81	0.98	0.75	0.87	0.77	0.93	0.76
Er [‡]	2.35	2.74	2.48	2.99	2.24	2.68	2.18	2.67	2.31
Tm [‡]	0.36	0.41	0.35	0.43	0.35	0.38	0.32	0.41	0.36
Yb [‡]	2.35	2.56	2.34	2.65	2.18	2.47	2.24	2.62	2.33
Lu [‡]	0.37	0.42	0.36	0.43	0.38	0.39	0.33	0.45	0.33
Mo [‡]	2	2	3	2	2	2	2	2	2
Pb [‡]	18	5	75	6	6	8	7	8	8
Tl [‡]	0.5	0.5	0.5	0.5	0.5	0.5	0.5	0.5	0.3
Na ₂ O/K ₂ O	2.29	1.29	1.48	2.52	1.91	3.16	1.75	1.78	1.66
Eu/Eu*	0.84	0.82	0.91	0.86	0.83	0.82	0.86	0.86	0.91
Corundum	0	0	0	0	0	0	0	0	0
Th/Ta	11.2	14.2	11.3	13.5	9.1	13.4	10.6	11.9	9.6
A/CNK	0.82	0.74	0.86	0.85	0.86	0.76	0.84	0.78	0.9
A/NK	2.38	2.48	2.20	2.10	2.20	2.17	2.34	2.34	2.12
[La/Yb] _N	3.13	3.4	2.77	3.59	4.24	3.14	4.21	3.04	4.31
Ta/Yb	0.13	0.16	0.13	0.15	0.14	0.12	0.13	0.11	0.17
Th/Yb	1.43	2.22	1.45	2.04	1.25	1.63	1.42	1.36	1.61
Th/Ta	11.17	14.23	11.30	13.53	9.07	13.40	10.57	11.87	9.62

[†]: measured by ICP-AES; [‡]: measured by ICP-MS

Intrusion	Neshveh unit									
	Quartz		Granodiorite						Granite	
Rock types	SN11	SK66	SK13	SN3	SN1	SN1	SN4	SN4	SN5	SK56
Sample	SN11	SK66	SK13	SN3	SN1	SN1	SN4	SN4	SN5	SK56
SiO ₂ [†]	59.6	60.8	62.1	62.3	62.5	62.7	64	65.1	69.4	71.2
TiO ₂ [†]	0.71	0.71	0.58	0.59	0.51	0.57	0.53	0.49	0.32	0.33
Al ₂ O ₃ [†]	16.7	15.7	16.8	15.7	15.4	16.1	15.6	14.8	13.8	12.7
Fe ₂ O ₃ [†]	7.66	7.66	4.96	5.98	5.07	6.03	5.17	3.89	3.05	3.05
MnO [†]	0.14	0.14	0.04	0.1	0.13	0.15	0.09	0.05	0.07	0.05
MgO [†]	2.48	2.41	2.52	2.58	2.05	1.78	1.98	1.52	1.1	0.6
CaO [†]	5.89	5.19	4.47	4.15	3.38	4.81	3.8	4.84	2.27	1.58
Na ₂ O [†]	3.59	3.44	4.99	3.36	3.64	3.49	3.41	3.47	3.06	2.56
K ₂ O [†]	2.31	2.38	1.57	2.95	3.46	2.73	3.26	2.9	4.19	5.14
P ₂ O ₅ [†]	0.2	0.22	0.19	0.19	0.15	0.19	0.16	0.15	0.09	0.11
Total	99.28	98.65	98.2	97.9	96.3	98.6	98.0	97.2	97.3	97.3
V [‡]	194	188	107	118	89	128	87	76	47	52
Cr [‡]	10	10	40	10	10	10	10	10	10	10
Ni [‡]	8	8	43	6	5	8	5	5	5	6
Co [‡]	17.4	16.6	11	12	8	12.8	10.2	5	4	5.5
Cu [‡]	48	29	44	59	22	47	17	5	8	25
Zn [‡]	75	65	26	40	80	76	51	23	44	40
Ga [‡]	17.7	16.3	17.3	15.3	15	16.2	15.3	14.4	13.2	12.9
Sn [‡]	1	2	2	1	1	1	1	2	1	1
W [‡]	2	3	1	2	2	2	2	1	1	1
Ba [‡]	548	605	380	618	701	675	665	759	808	500
Sr [‡]	424	394	525	381	347	449	352	353	248	145
Rb [‡]	60.9	56	44.2	63.5	74.2	71.4	78.2	38.1	90.8	201
Nb [‡]	6.6	6.6	11.6	6.5	7.9	6.6	8.2	7.4	8.7	9.9
Y [‡]	23	25.7	14.1	17.5	21.6	20.4	19.7	18.4	16.2	23.2
Zr [‡]	119	145	151	113	134	121	145	145	124	189
Cs [‡]	2.34	1.88	2.35	1.19	1.49	1.22	1.74	0.4	1.47	3.07
Hf [‡]	3.5	4.2	3.7	3.1	3.8	3.6	4.1	4.1	3.8	6.2
Ta [‡]	0.5	0.4	0.8	0.5	0.5	0.5	0.5	0.5	0.7	0.8
Th [‡]	5.11	4.62	7.12	4.98	5.89	5.55	6.18	5.91	8.42	21.1
U [‡]	1.23	1.47	1.93	1.05	1.3	1.43	0.97	1.56	1.78	5.18
La [‡]	15.3	16.5	20.2	13.1	16.8	24.2	13.1	16	19.7	19.9
Ce [‡]	30.8	33.3	35.9	25.6	32.6	45.7	26.6	31.6	34.9	38.1
Pr [‡]	3.85	4.16	3.99	3.3	4.07	5.24	3.53	3.85	3.9	4.39
Nd [‡]	15.4	16.8	14	13.3	16.2	19.3	14.2	14.9	14.2	16.3
Sm [‡]	3.53	4.02	2.68	3.1	3.7	3.76	3.43	3.21	2.84	3.54
Eu [‡]	0.94	1.04	0.8	0.98	0.91	0.95	0.9	0.88	0.6	0.51
Gd [‡]	3.87	4.4	2.92	3.4	4.15	3.91	3.69	3.65	2.99	3.85
Tb [‡]	0.62	0.69	0.42	0.54	0.64	0.56	0.59	0.55	0.46	0.63
Dy [‡]	4	4.44	2.51	3.22	3.88	3.48	3.56	3.26	2.8	4.03
Ho [‡]	0.8	0.94	0.51	0.66	0.83	0.71	0.74	0.69	0.6	0.85
Er [‡]	2.45	2.76	1.45	1.99	2.41	2.12	2.28	2.12	1.89	2.57
Tm [‡]	0.34	0.42	0.21	0.29	0.37	0.32	0.34	0.32	0.29	0.38
Yb [‡]	2.39	2.68	1.39	1.93	2.44	2.14	2.29	2.16	2.06	2.65
Lu [‡]	0.4	0.47	0.21	0.29	0.37	0.36	0.36	0.33	0.34	0.44
Mo [‡]	2	2	2	2	2	2	2	2	2	2
Pb [‡]	11	12	6	10	21	13	15	6	17	11
Tl [‡]	0.5	0.5	0.5	0.5	0.5	0.5	0.5	0.5	0.5	0.5
Na ₂ O/K ₂ O	1.55	1.45	3.18	1.14	1.05	1.28	1.05	1.2	0.73	0.5
Eu/Eu*	0.78	0.76	0.87	0.92	0.71	0.76	0.77	0.79	0.63	0.42
Corundum	0	0	0	0	0	0	0	0	0.31	0.31
Th/Ta	10.2	11.6	8.9	10	11.8	11.1	12.4	11.8	12	26.4
A/CNK	0.87	0.89		0.97	0.97	0.93	0.98	0.84	1.01	1
A/NK	1.99	1.91	1.7	1.81	1.59	1.86	1.71	1.67	1.44	1.3
[La/Yb] _N	4.32	4.15		4.58	4.64	7.62	3.86	4.99	6.45	5.06
Ta/Yb	0.21	0.15	0.58	0.26	0.2	0.23	0.22	0.23	0.34	0.3
Th/Yb	2.14	1.72	5.12	2.58	2.41	2.59	2.7	2.74	4.09	7.96
Th/Ta	10.22	11.55	8.9	9.96	11.7	11.1	12.3	11.8	12.0	26.3

Intrusion	Selijerd unit						
Rock type	Granodiorite						
Sample	SS23	R7	SS56	SS54	SS57	SS58	SS61
SiO ₂ [†]	63.3	65.5	67.4	67.5	67.6	68.6	68.9
TiO ₂ [†]	0.81	0.71	0.68	0.65	0.7	0.71	0.66
Al ₂ O ₃ [†]	14.7	15.3	15.25	14.9	14.65	14.9	14.55
FeO [‡]		5.34					
Fe ₂ O ₃ [†]	6.95		4.8	5.1	5.21	5.26	5.04
MnO [‡]	0.13	0.11	0.07	0.07	0.09	0.07	0.07
MgO [†]	2.09	1.78	1.44	1.43	1.68	1.62	1.36
CaO [†]	5.28	5.09	4.55	4.39	4.33	4.07	3.91
Na ₂ O [†]	3.43	4.23	4.89	4.45	4.47	4.84	4.24
K ₂ O [†]	2.12	1.09	1.07	1.41	1.52	1.3	1.54
P ₂ O ₅ [†]	0.19	0.17	0.14	0.15	0.17	0.16	0.14
Total	99.0	99.3	100.2	100.0	100.4	101.5	100.4
V [‡]	117	123	80	74	81	84	66
Cr [‡]	10	20	10	10	10	10	10
Ni [‡]	5	20	5	5	5	6	5
Co [‡]	13.2	8	5.4	6.7	7	5.4	4.7
Cu [‡]	13	10	5	7	11	7	5
Zn [‡]	62	30	36	33	35	30	35
Ga [‡]	16.3	17	17.4	17.2	16.6	16.6	16.9
Sn [‡]	2	8	2	2	1	1	1
W [‡]	1	1	1	1	1	1	1
Ba [‡]	471	386	421	572	442	426	534
Sr [‡]	223	216	217	202	199.5	209	217
Rb [‡]	33.1	11	11.2	18.9	16.6	14.9	19.4
Nb [‡]	8.9	5.7	8.5	8.6	8.1	8.6	9.2
Y [‡]	37.6	38.5	34.6	40.2	35.3	33.6	35.8
Zr [‡]	157	77	132	153	127	138	137
Cs [‡]	0.31	0.1	0.15	0.13	0.21	0.17	0.19
Hf [‡]	4.9	2.7	3.9	4.4	3.9	4.2	4
Ta [‡]	0.6	0.37	0.5	0.5	0.5	0.5	0.6
Th [‡]	5.33	3.72	2.18	3.37	3.28	2.77	4.89
U [‡]	1.39	1.29	0.49	0.94	0.75	0.72	0.97
La [‡]	21.1	18.2	8.9	10.4	10.4	9.7	8.6
Ce [‡]	42.2	35.5	21.3	26	23.1	19.3	20.1
Pr [‡]	5.39	4.44	3.21	3.92	3.42	2.94	3.04
Nd [‡]	22.3	18.3	15	18.3	15.3	13.9	14.2
Sm [‡]	5.58	4.7	4.31	5.34	4.38	4.11	4.25
Eu [‡]	1.32	1.25	1.29	1.47	1.22	1.17	1.21
Gd [‡]	6.25	6.02	5.13	6.25	5.37	5.07	5.14
Tb [‡]	1.1	1.16	0.98	1.15	0.97	0.94	0.98
Dy [‡]	6.85	6.85	6.27	7.28	6.36	5.93	6.3
Ho [‡]	1.48	1.44	1.39	1.61	1.4	1.34	1.38
Er [‡]	4.39	4.46	4.09	4.99	4.19	4.01	4.15
Tm [‡]	0.65	0.66	0.62	0.73	0.63	0.6	0.64
Yb [‡]	4.36	3.9	3.93	4.83	4.27	3.96	4.2
Lu [‡]	0.65	0.65	0.62	0.74	0.67	0.62	0.64
Mo [‡]	6	2	2	2	2	2	2
Pb [‡]	6	6	6	5	5	8	6
Tl [‡]	0.5	0.5	0.5	0.5	0.5	0.5	0.5
Na ₂ O/K ₂ O	1.62	3.88	4.57	3.16	2.94	3.72	2.75
Eu/Eu*	0.68	0.72	0.84	0.78	0.77	0.78	0.79
Corundum	0	0	0	0	0	0	0
Th/Ta	8.9	10.1	4.4	6.7	6.6	5.5	8.2
A/CNK	0.84	0.88	0.87	0.89	0.87	0.89	0.92
A/NK	1.86	1.88	1.66	1.68	1.63	1.59	1.68
[La/Yb] _N	3.26	3.15	1.53	1.45	1.64	1.65	1.38
Ta/Yb	0.14	0.09	0.13	0.10	0.12	0.13	0.14
Th/Yb	1.22	0.95	0.55	0.70	0.77	0.70	1.16
Th/Ta	8.88	10.0	4.36	6.74	6.56	5.54	8.15

For Selijerd unit, Fe₂O₃, MgO, MnO, CaO, P₂O₅, La, Ce, Co and V show linear descending trends

versus SiO₂, whereas Na₂O and Nb increase with increasing SiO₂ content (Figs. 5, 6). The variations

of some trace elements (e.g., Cs) for all three units show scattering with no significant trends with increasing SiO₂. Compared to the Khalkhab and Neshveh rocks, the Selijerd granodioritic rocks with similar SiO₂ values are richer in TiO₂, CaO, NaO₂, Y and poorer in K₂O, Cs, Rb, Ba, La, Th and

Sr (Figs. 5, 6; Table 1). This evidence suggests a chemical affinity and a probable genetic relationship between the Khalkhab and Neshveh (KN) units, whereas the Selijerd unit seems to be derived from a different source or has experienced a different magmatic differentiation trend.

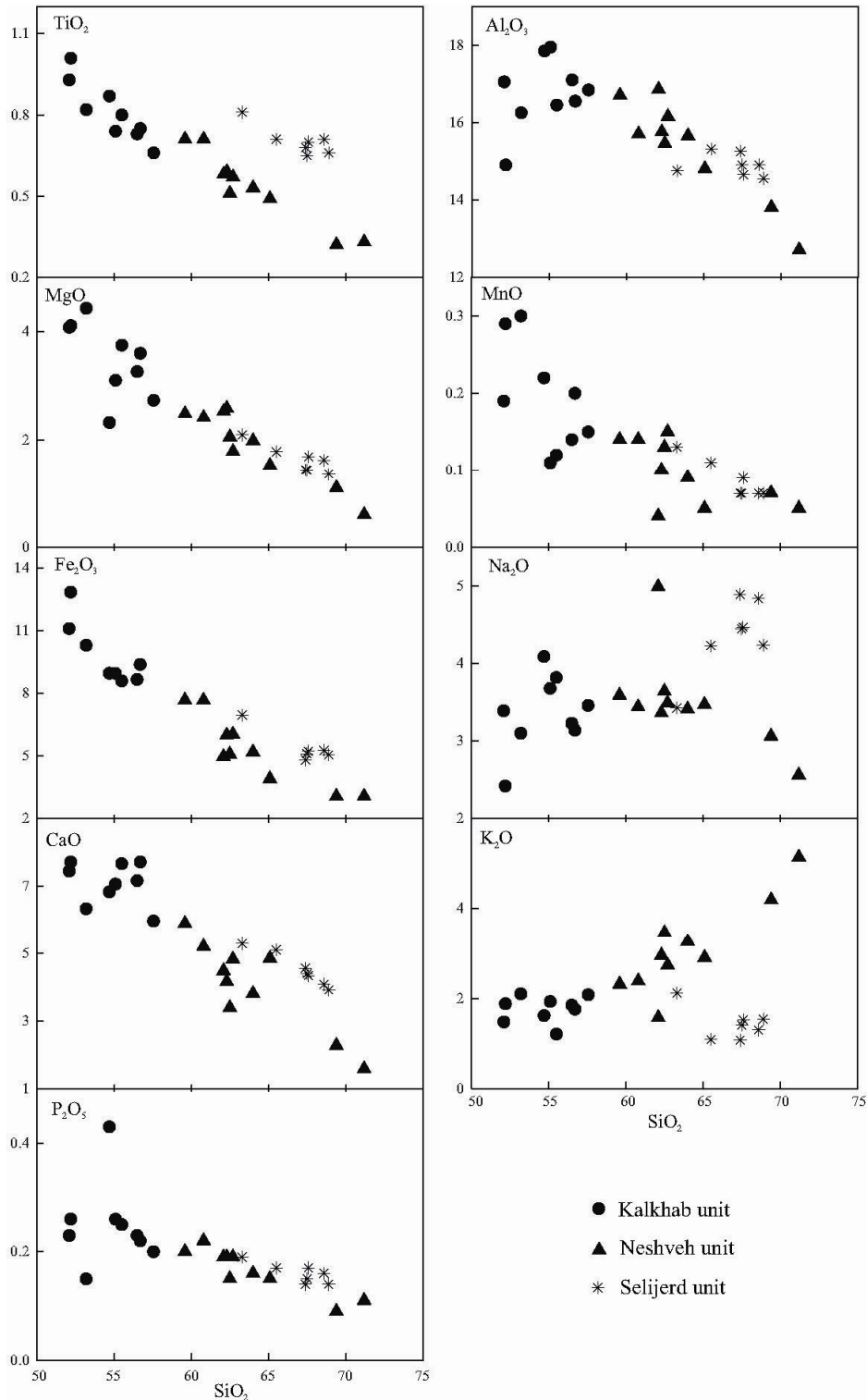


Figure 5: Selected major oxides vs. SiO₂ (wt%) content for the northwest Saveh intrusive rocks

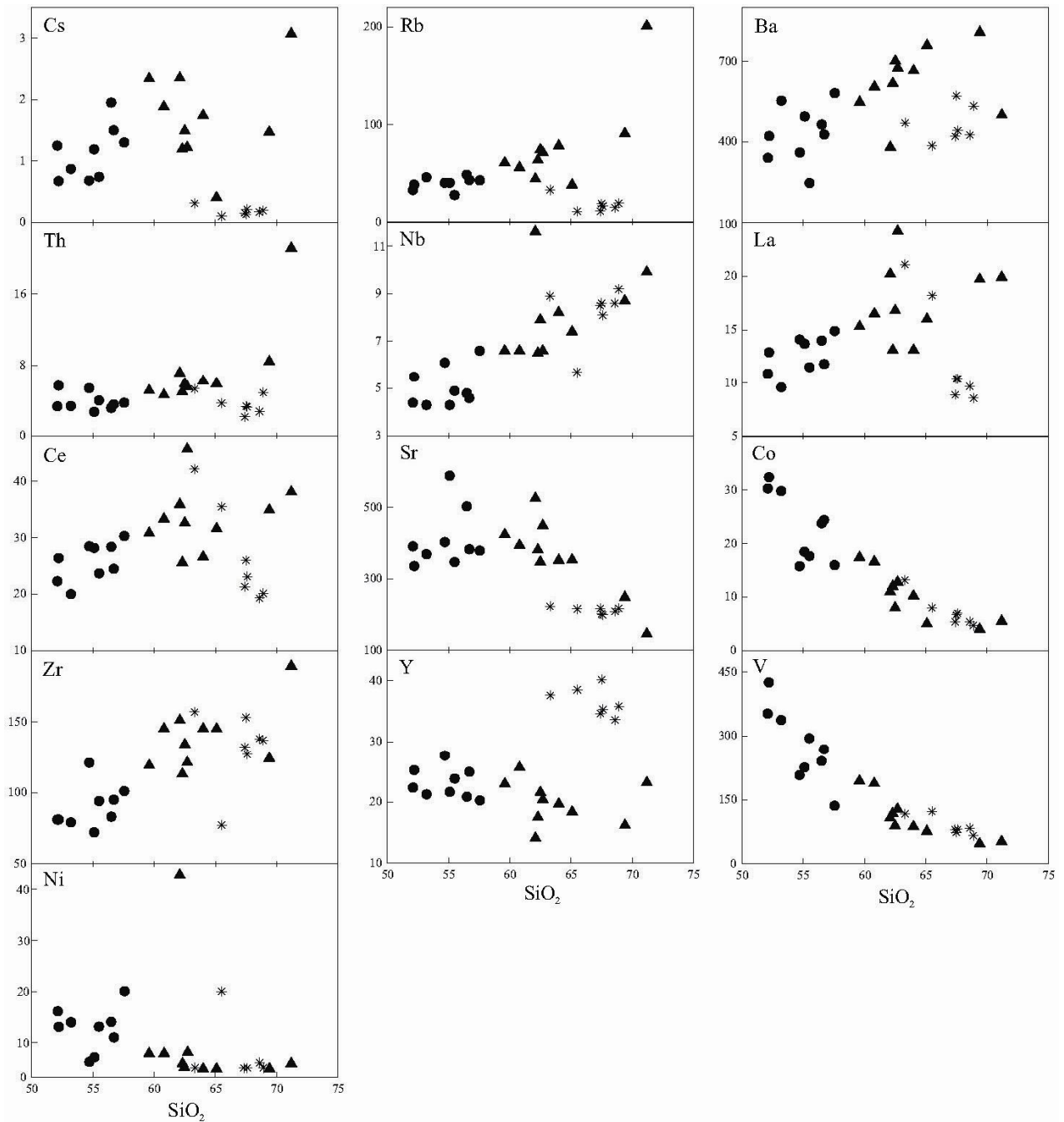


Figure 6: Selected trace elements (ppm) vs. SiO₂ (wt%) content for the northwest Saveh intrusive rocks (Symbols are the same as Fig. 5.)

Both Khalkhab quartz monzodioritic and Neshveh granodioritic samples plot in the medium to high K fields on the K₂O versus the SiO₂ diagram (Rickwood, 1989) Fig. 7, while the Selijerd rocks plot into the low- to medium-K domain and have tholeiitic to calc-alkaline characteristics (Fig. 7). All samples show high Na₂O/ K₂O ratios (0.5- 8.46), and plot into the metaluminous field in the Al₂O₃/(CaO + Na₂O+K₂O) versus Al₂O₃/(Na₂O+K₂O) [A/CNK vs.

A/NK] diagram (Fig. 8)(Shand, 1943).

Chondrite-normalized Rare Earth Element (REE) patterns for the northwest Saveh intrusions are shown in figure 9A, using the chondrite values of Boynton (1984). The Light Rare Earth Element (LREE) patterns show 30-50 times the chondrite values for the Khalkhab unit, 40-80 times for the Neshveh unit and 30-70 times for the Selijerd unit.

The studied granitoid rocks exhibit slightly fractionated REE patterns ([La/Yb]_N = 3.4, 5.48

and 1.99 for the Khalkhab, Neshveh and Selijerd units, respectively), variable Eu anomalies ($Eu/Eu^* = 0.82-0.91, 0.42-0.92$ and $0.68-0.84$ for the Khalkhab, Neshveh and Selijerd units, respectively), and flat heavy HREE patterns. Some of the Neshveh granitoid rocks show highly negative Eu anomalies ($Eu/Eu^* = 0.42-0.92$) whereas the Selijerd samples have the flatter REE patterns.

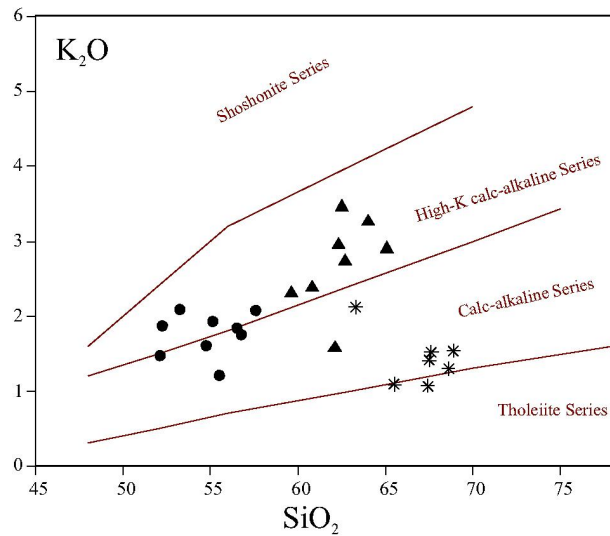


Figure 7: A plot of K_2O vs. SiO_2 for the northwest Saveh intrusive rocks (Rickwood 1989) (Symbols are the same as Fig. 5.)

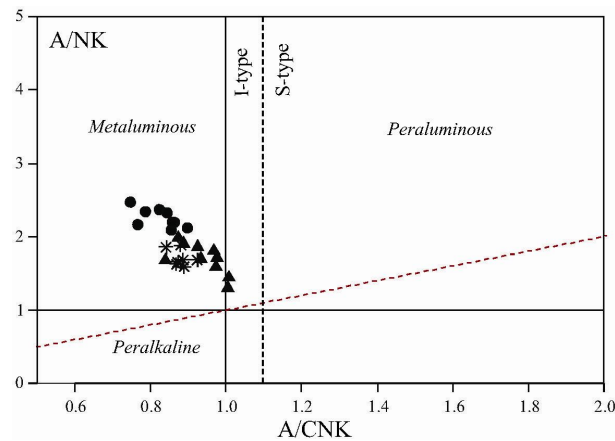


Figure 8: A/NK (molar ratio $Al_2O_3/(Na_2O+K_2O)$) vs. A/CNK (molar ratio $Al_2O_3/(CaO + Na_2O+K_2O)$) diagram for the northwest Saveh intrusion rocks (Shand, 1943) (The I & S boundary is after Chappell (1999). Symbols are the same as Fig. 5.)

Trace element distribution patterns for the northwest Saveh intrusions are normalized to lower continental crust in Figure 9B, following Taylor and McLennan (1985). Most of the study samples show Nb and Ti depletions and are enriched in Th

and K. In comparison with high field strength elements (HFSEs: Nb, Ta, Hf, Zr, Sm, Y, and Yb), Large Ion Lithophile Elements (LILEs: Cs, Rb and Ba) show enrichment.

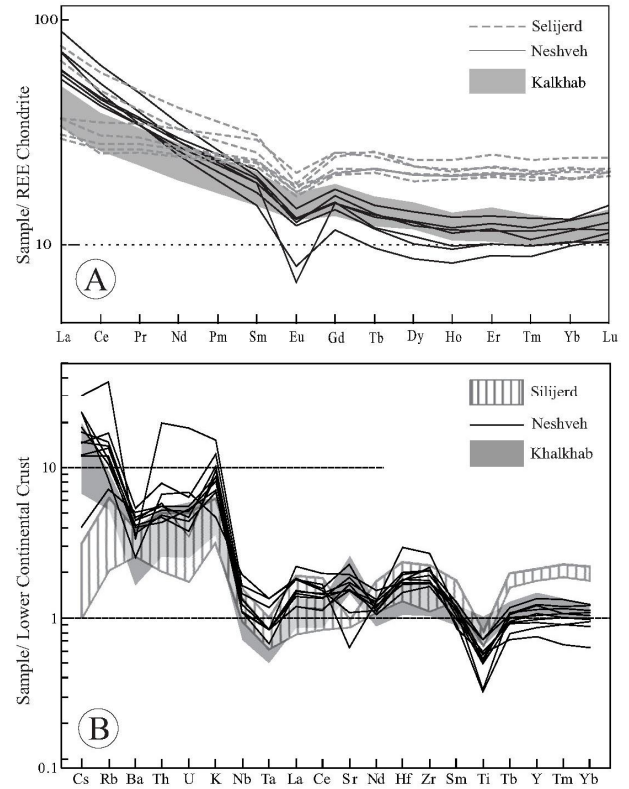


Figure 9: A. Chondrite normalized rare earth element plot of the northwest Saveh rocks. B. Lower continental crust normalized trace element patterns. Normalization values are after Boynton (1984) and Taylor and McLennan (1985), respectively.

Sr and Nd isotopes

Six representative samples (four from the Khalkhab and Neshveh units and two from the Selijerd unit) were selected for determination of $^{143}Nd/^{144}Nd$ and $^{87}Sr/^{86}Sr$ isotopic ratios (Table 2). The rocks from the Khalkhab unit generate an isochron (MSWD = 0.26), but with a very high error in the age (15.3 ± 8 Ma) due to a small range in $^{87}Rb/^{86}Sr$ ratio (Fig. 10). U–Pb zircon dating by Rezaei-Kahkhaei (2011) confirms a 39 Ma age for the northwest Saveh intrusions. Thus, initial isotope values are calculated at 39 Ma (Table 2). $^{87}Sr/^{86}Sr_{39}$ ranges from 0.704536 to 0.70486, with an average of 0.704705 and $(^{143}Nd/^{144}Nd)_{39}$ ranges from 0.5127 to 0.51279 with an average of 0.51274. These initial Sr and Nd isotopic ratios from northwest Saveh intrusions plot into the upper left quadrangle of the Sr-Nd diagram corresponding to upper mantle

signatures (Fig. 11). They also plot close to each other, suggesting a genetic link between different rock types in the study area, or at least similar sources.

Table 2: The Sr-Nd isotopic data of the northwest Saveh intrusive rocks. $^{87}\text{Sr}/^{86}\text{Sr}$ initial ratios and ϵ_{Nd} values calculated for $t=15$ Ma.

Pluton name	Khalkhab		Neshveh		Selijerd	
	Quartz monzogabbro		Granodiorite		Tonalite	Granodiorite
Sample No	SS2	SK18	SK47	SN15	SS23	SS61
SiO ₂ (wt%)	51.4	53.2	60.5	62.7	63.3	68.9
Rb	3.7	46.3	107.5	69.8	35	20.2
Sr	400.2	373.3	356	443.6	230.8	222.7
Rb/Sr	0.009	0.124	0.302	0.157	0.152	0.091
$^{87}\text{Rb}/^{86}\text{Sr}$	0.0267	0.3587	0.8734	0.4551	0.4386	0.2624
$^{87}\text{Sr}/^{86}\text{Sr}$	0.704853	0.704901	0.705033	0.704830	0.705	0.705009
$(^{87}\text{Sr}/^{86}\text{Sr})_i$	0.704838	0.704697	0.704536	0.704570	0.704728	0.704860
Sm	1.762	2.714	3.164	3.468	5.058	3.703
Nd	6.163	10.041	13.724	17.588	20.154	12.292
Sm/Nd	0.286	0.27	0.231	0.197	0.251	0.301
$^{147}\text{Sm}/^{144}\text{Nd}$	0.1728	0.1634	0.1394	0.1192	0.1517	0.1821
$^{143}\text{Nd}/^{144}\text{Nd}$	0.51277	0.512797	0.512825	0.51277	0.5128	0.512748
$(^{143}\text{Nd}/^{144}\text{Nd})_i$	0.51273	0.51276	0.51279	0.51273	0.51273	0.51270
ϵ_{Nd_i}	2.7	3.3	3.9	2.9	2.8	2.2
T _{DM}	608	562	510	595	603	645

The decay constants used in the calculations are $\lambda^{87}\text{Rb}=1.42\times 10^{-11}$ and $\lambda^{147}\text{Sm}=6.54\times 10^{-12}$ year⁻¹ recommended by the IUGS Sub-commission for Geochronology (Steiger and Jäger, 1977). Analytical uncertainties are estimated to be 0.01% for $^{87}\text{Sr}/^{86}\text{Sr}$ ratios and 0.006% for $^{143}\text{Nd}/^{144}\text{Nd}$ ratios and 1% and 0.1% for the $^{87}\text{Rb}/^{86}\text{Sr}$ and $^{147}\text{Sm}/^{144}\text{Nd}$ ratios respectively. Epsilon Nd (ϵ_{Nd}) values were calculated relative to a chondrite present day: $(^{143}\text{Nd}/^{144}\text{Nd})_{\text{todayCHUR}}=0.512638$; $(^{143}\text{Sm}/^{144}\text{Nd})_{\text{todayCHUR}}=0.1967$. t =time used for the calculation of the isotopic initial ratios. The age (39Ma) is the calculated in this work. T_{DM} is two-stage mantle model age after DePaolo *et al.* (1991).

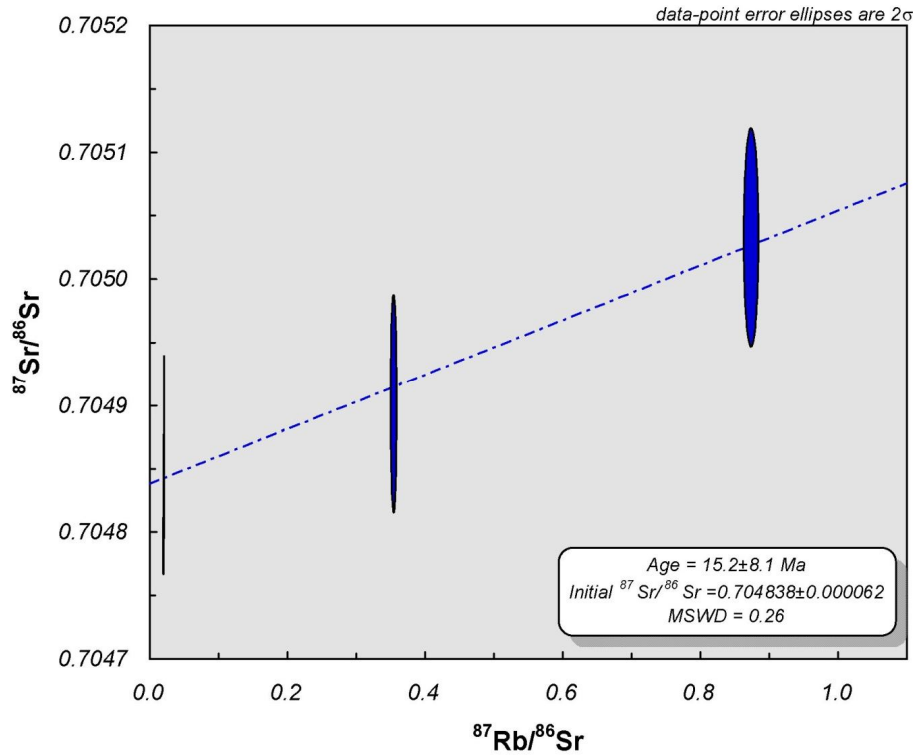


Figure 10: Rubidium–strontium isotopic data for whole rock from the KN units. Three data points define a linear array corresponding to a Rb–Sr age of 15.2 ± 8Ma with an initial $^{87}\text{Sr}/^{86}\text{Sr}$ = 0.704838 ± 0.000062 (MSWD=0.26).

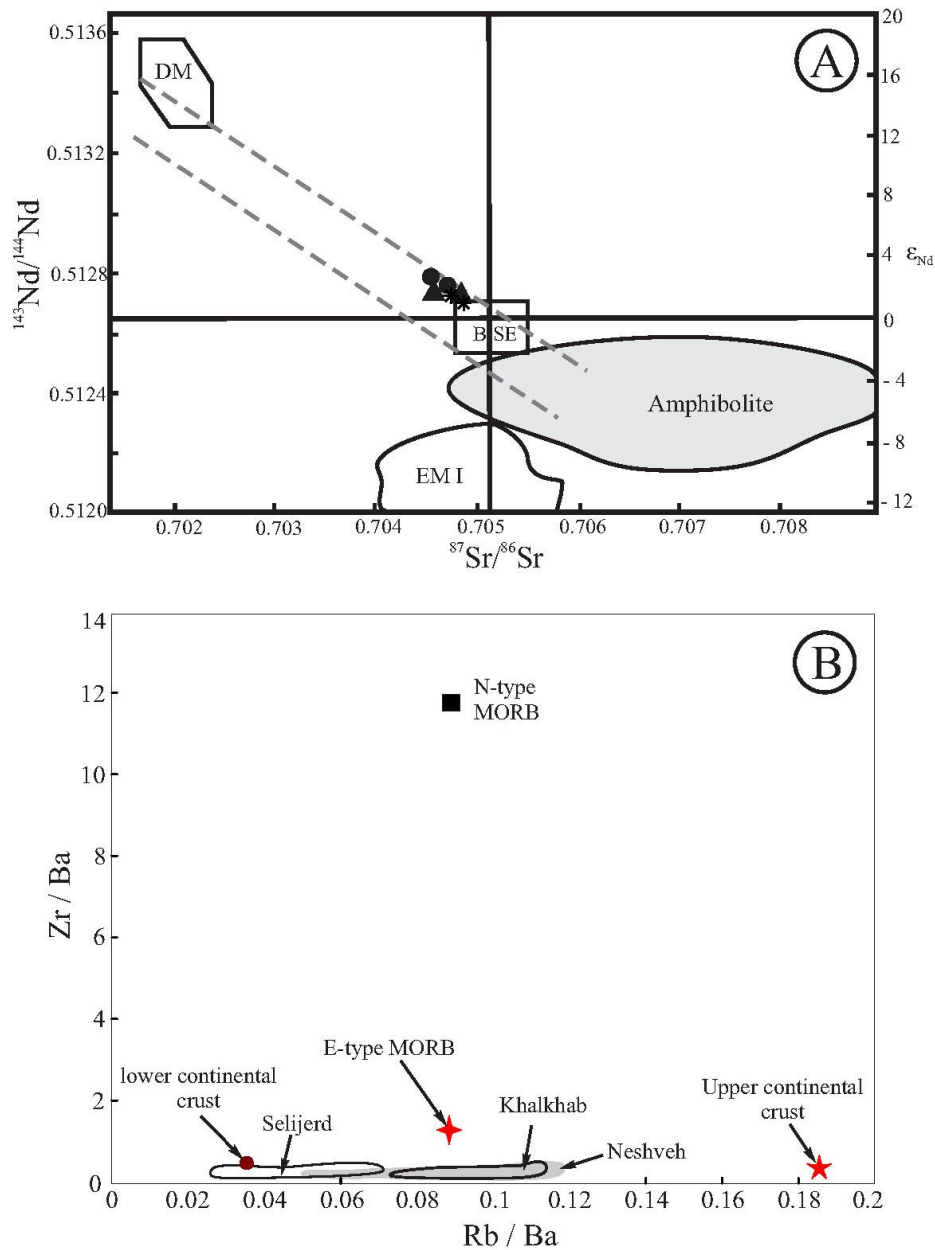


Figure 11: A. ϵ_{Nd} vs. ($^{87}Sr/^{86}Sr$); for the northwest Saveh intrusive rocks. Initial isotope ratios are calculated at an age of 15 Ma. BSE=Bulk Silicate Earth (after Rollinson 1993). Amphibolite area is from Kohut and Nabelek (2008). B. Zr/ Ba vs. Rb/ Ba diagram for the northwest Saveh intrusive rocks (this paper), N-type mantle, E-type mantle, lower continental crust and upper continental crust (after Sun and McDonough 1989). It represents that the study rocks plot near E-type mantle and lower continental crust components. Symbols are the same as Fig. 5.

Discussion

Fractional crystallization processes

Some workers suggest that the existence of a wide range of plutonic rocks, showing linear patterns in major and trace element plots, might have resulted from the mixing of mafic and felsic components (e.g., Popov *et al.*, 1999; Bea *et al.*, 2005), or by combined processes of fractional crystallization and assimilation (DePaolo, 1981; Spera & Bohrsen, 2001; Thompson *et al.*, 2002; Kuritani *et al.*, 2005).

These hypotheses can be tested by field, petrographic and geochemical studies. The linear patterns of major and trace elements in the Khalkhab and Neshveh units, can most likely be explained by fractional crystallization and local assimilation, because: (1) all rocks have approximately the same initial $^{87}Sr/^{86}Sr$ and $^{143}Nd/^{144}Nd$ ratios (Table 2) and hence might share a common magma source, (2) according to Chappell (1996) mixing and/or mingling and

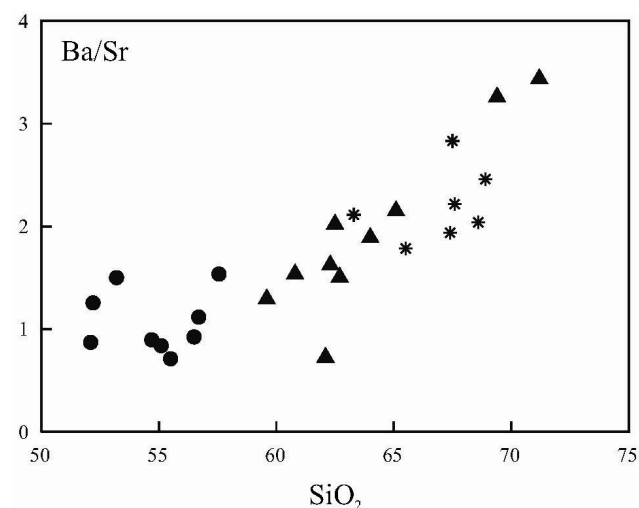
assimilation may be locally significant but cannot be invoked to account for large-scale compositional variations, and (3) although magma mixing is probably the major cause of linear variation in major and trace element Harker diagrams, it never explains inflections in magmatic trends such as those that appear in the KN rocks (e.g., Na₂O and Sr) (Figs. 5, 6).

Whole-rock geochemical variations along the Khalkhab and Neshveh traverses are best marked by SiO₂, which increases from about 52.1 wt.% in the west to 69.1 wt.% in the east (Table 1; Fig. 2). Chemical data agree with petrographic results as the whole plutonic ensemble ranges from quartz monzogabbro and quartz monzodiorite in the west to granite in the east (Fig. 2).

Decreasing of TiO₂, Al₂O₃, MgO, Fe₂O₃ and CaO, and increasing of K₂O and Rb with increasing SiO₂ (Figs. 5, 6) can be interpreted by the fractionation of clinopyroxene, hornblende, plagioclase, titanite and possibly magnetite (Wilson, 2007). A decrease in P₂O₅ with an increase in SiO₂ can be interpreted as apatite saturation that subsequently led to apatite fractionation (Chappell & White, 1992). Na₂O abundances show an inflected trend with increasing SiO₂, suggesting that plagioclase did not crystallize until the melt reached the point of SiO₂ = 55 wt%. Sr substitutes for Ca in plagioclase rather than clinopyroxene, and shows the same trend in the Khalkhab and Neshveh rocks with a positive correlation up to SiO₂ = 55 wt% and then a negative correlation. Therefore, Na₂O and Sr inflections may indicate that plagioclase did not fractionate from the magma until the silica value in the melt reached SiO₂ = 55 wt%.

Zr concentration in magmas may be controlled by zircon saturation (Hoskin, 2000). Thus, it can be concluded that Zr contents might reach saturation values in granitic rocks, which is consistent with zircon paucity in quartz monzogabbro, quartz monzodiorite and granodiorite. Sr is incompatible for most common minerals except plagioclase and Ba are similarly partitioned in K-feldspar. Therefore, Ba/Sr ratios increase with crystallization of plagioclase, but decrease when K-feldspar begins to crystallize. Ba/Sr ratios show an increasing trend during the magmatic fractionation for the Khalkhab and Neshveh rocks because of plagioclase fractionation (Fig. 12). Co and V show a pronounced negative correlation with silica

content and behave as compatible elements. The decrease in V and TiO₂ together with increasing SiO₂ (Figs. 5, 6) provides evidence for the fractionation of Fe-Ti oxides (Omrani *et al.*, 2008).



Neshveh rocks in comparison with the Khalkhab samples shows that fractionation of plagioclase had an important role in the evolution of parent magma towards the formation of Neshveh rocks. This in turn justifies the Na₂O and Sr inflection trends of the Harker variation diagrams from the Khalkhab and Neshveh (KN) rocks.

The KN rocks are enriched in large-ion lithophile (LIL) elements (e.g., Cs, Ba, Rb, U, K), relative to high-field-strength (HFS) elements (e.g., Nb, Zr and Y; Fig. 9B), and have significant depletions in Nb and Ti. These characteristics suggest some upper crustal assimilation during magmatic evolution and/or display the signature of a subduction component, i.e., fluids (or melts) derived from the subducted sediments (Sun & McDonough, 1989). The negative anomalies of Nb-Ta are typical for calc-alkaline magmas formed above a subduction zone (Saunders & Tarney, 1979; Pearce, 1982; McCulloch & Gamble, 1991; Tatsumi & Eggins, 1995; Wilson, 2007). The wide variations in the abundances of Nb, Ta and Th (4.3–11.6 ppm, 0.3–0.8 ppm, 1.18–21.1 ppm, respectively) are also key features of the KN rocks that were the result of fractional crystallization.

The important feature of the Selijerd samples is the flat REE patterns from LREE to HREE (Fig. 9A), which is a significant feature of tholeiitic magmas (Fujinawa, 1992; Tatsumi, 2009). This is also confirmed by the plotting of Selijerd samples into the tholeiitic and calc-alkaline fields of a Rickwood (1989) diagram (Fig. 7); and higher TiO₂ and Fe₂O₃ contents in comparison with the Khalkhab and Neshveh units which plot in high-K calc-alkaline field. Samples SS23 and R7 are richer in LREE than the other Selijerd samples. This enrichment might be caused by the contamination of country rocks, since they are located close to the pluton margin (Fig. 2).

The negative Ti anomaly in the northwest Saveh intrusive rocks (Figs. 9b) is consistent with titanite and Fe-Ti oxide (e.g., titanomagnetite) fractionation, respectively, suggesting an origin related to a subduction process (Mitropoulos *et al.*, 1987).

Source rock materials

According to Chappell and White (1974) and White and Chappell (1983) the northwest Saveh rocks show I-type characteristics. They have key I-type modal minerals (clinopyroxene, hornblende,

magnetite and titanite). This is also confirmed by geochemical data such as relatively low SiO₂ (61.62 wt% in average), relatively high Na₂O contents (~3.69 wt% in average), low molecular A/CNK ratio (<1.1), Na₂O/ K₂O ratios (~2.06 in average), and low normative corundum contents (< 1%; Table 1).

Despite the different petrographic and geochemical characteristics of the northwest Saveh intrusions, they have a similar initial Sr and Nd isotopic ratios, which suggest that all the rock types were genetically derived from the same source materials. They are characterized by low initial ⁸⁷Sr/⁸⁶Sr ratios (0.704536 to 0.70486; Fig. 10; Table 2) and high initial ¹⁴³Nd/¹⁴⁴Nd ratios (0.5127 to 0.51279) and plot on the left side of bulk silicate Earth in the mantle array (Fig. 11A). Considering the following points might be good to find out a suitable source for the northwest Saveh intrusions. (1) The same initial isotopic ratios of ⁸⁷Sr/⁸⁶Sr and ¹⁴³Nd/¹⁴⁴Nd in the quartz monzogabbros and granodiorites. (2) The same origin for quartz monzogabbros and granodiorites. Thus, it seems that quartz monzogabbros, which are intermediate in composition, are more suitable to find out the source of studied rocks, and this can be used to for justification of the other rock types.

There are many ways to make intermediate rocks. Endmember hypotheses for the origin of intermediate rocks are: (1) direct melting of the mantle at water-saturated conditions, (2) partial re-melting of altered basaltic crust, (3) mixing of mafic magmas with high Si crust or magmas, e.g., dacite-rhyolite, and (4) crystal fractionation of arc basalts in crustal magma chambers.

A 10–20% melt of an upper mantle with 5 ppm Zr and 0.019 wt.% P₂O₅, equivalent to that estimated for depleted mid-ocean ridge basalt mantle (Workman and Hart, 2005), yields primary liquids with 25–50 ppm Zr and 0.1–0.2 wt.% P₂O₅. These levels are lower than intermediate magmas (here studied quartz monzogabbro having 87 ppm Zr and 0.26 P₂O₅ in averages; Table 1). Thus, direct melting of the mantle at water-saturated conditions may not be a suitable mechanism for generating the studied rocks. Indeed, the only intermediate magmas, which have sufficiently low Zr and P, are those basaltic andesites and andesites identified boninites, which have a high Mg# (where Mg# = atomic Mg/(Mg+ Fe_T) and Fe_T represents total Fe).

Making intermediate rocks by re-melting the

basaltic lower crust has been shown to be energetically unfavourable (Dufek & Bergantz, 2005). Generating intermediate rocks by crystal-liquid segregation, while energetically simpler, is faced with the problem of how to efficiently separate such viscous liquids from the crystals.

Recently Lee and Bachmann (2014) studied the genesis of intermediate magmas by using 7382 samples from the subduction zones of Mariana Island arc, Peninsular Ranges batholith in California, the southern Andes, and the Aegean arc in Europe. They pointed out that no more than ~20% of the intermediate continental arc and none of the island arcs fall on pure end-member mixing arrays between basalt and rhyolite, indicating the mixing of mafic magmas with high Si crust or magmas is not the dominant process in the generation of intermediate magmas.

Finally, it seems that crystal fractionation of arc basalts in crustal magma chambers is a suitable mechanism of the generation of the parent magmas in the northwest Saveh intrusions. In this way, high-pressure crystal fractionation of hydrous basalts, coupled with some lower crustal assimilation early in the differentiation process - prior to silica enrichment- is a fundamental mechanism for the parent magmas of quartz monzogabbros. This, of course, enables the formation of large volumes of mafic and ultramafic cumulates in the lower crust. Consequently, we speculate that granodiorites from the northwest Saveh intrusions formed dominantly by crystal fractionation from evolved parent magmas that have ascended into the upper crust. Such a model is consistent with the few crustal cross-sections sampled at the surface of our planet (Jagoutz & Schmidt, 2012; Greene *et al.*, 2006; Otamendi *et al.*, 2012). Occurrence of crustal contamination early in the magmatic differentiation process is also supported by similar isotopic ratios of Sr and Nd in mafic and felsic endmembers.

The Selijerd unit has low- to medium-K levels and a low initial $^{87}\text{Sr}/^{86}\text{Sr}$ (0.70473-0.70486). Previous researchers (Johnston & Wyllie, 1988; Beard & Lofgren, 1991; Rapp *et al.*, 1991; Beard *et al.*, 1994; Wolf & Wyllie, 1994; Tupinambá *et al.*, 2012) showed that partially-melted low and medium K basic and intermediate magma generally produce tonalitic and granodioritic magma that are poorer in K levels than common granodiorites and granites. The Selijerd rocks show flat patterns on

chondrite-normalized REE plots compared with the other Saveh intrusions, reflecting the complexity of the magmatic processes including variation in the depth and degree of partial melting, magma mixing, fractionation and assimilation in subduction zones.

The geodynamic setting partly controls the type of source rocks at depth. Thus, the igneous composition indirectly gives information about the geodynamic setting. For this reason, the Ta/Yb–Th/Yb geodynamic discrimination diagram of Gorton and Schandl (2000) was used for the northwest Saveh units. The studied samples are plotted in the active continental margin field (Fig. 13) and were probably generated in a subduction zone during the convergence of the Arabia and Iran plates. They are also enriched in LIL elements such as K, Pb and Sr, and depleted in HFS elements (e.g., Nb, Zr and Y) with Nb and Ti anomalies (Fig. 9b) observed in active continental margin environments. The average ratios of Th/Ta from the northwest Saveh rocks are 10.8, supporting this statement (Table 1; Gorton & Schandl, 2000). These results are consistent with the subduction setting for the UDMA proposed by previous workers (Omran *et al.*, 2008; Arvin *et al.*, 2007).

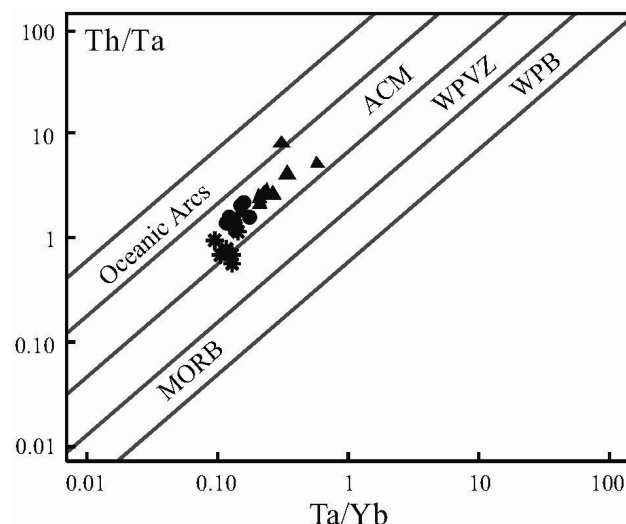


Figure 13: Th/Yb – Ta/Yb discrimination diagram after Gorton & Schandl (2000) shows an active continental margin (ACM) for the northwest Saveh intrusions. Other abbreviations are: WPVZ= within-plate volcanic zones; MORB= mid oceanic ridge basalt. Symbols are the same as Fig. 5.

Conclusion

The northwest Saveh intrusions are made of various I-type granitoid plutons, ranging from quartz monzogabbro to granite. The main rock types can be divided into three groups: the Selijerd

granodiorite unit, the Khalkhab quartz monzodiorite unit and the Neshveh granodiorite unit. The Khalkhab and Neshveh units form an elongated body from west to east and share similar geochemical characteristics, whereas the Selijerd unit shows a different magmatic character. Detailed geochemical data reveal that the Selijerd unit has a chemical and mineralogical zoned structure that becomes progressively more felsic towards the central intrusion. Major elements, Th, La, Ce, V and Co decrease, while SiO₂ and N₂O increase from the margin to the centre of the pluton. Alkali feldspar and quartz become more abundant in inner zones, and plagioclase, amphibole and Fe-Ti oxides decrease outward. The Khalkhab and Neshveh rocks show gentle differentiation trends, where most major (Al₂O₃, Fe₂O₃, MgO, CaO, TiO₂, and P₂O₅) and trace (Sr, Co, V, and Ni) elements are negatively correlated with SiO₂. K₂O and Ba, Rb, Ce, Nb, Zr are positively correlated with SiO₂. Some elements (Na₂O and Sr) define broken lines

on Harker variation diagrams where positive up to SiO₂ = 55 wt%, and turn into negative correlation for SiO₂ > 55 wt % (Figs. 5 and 6). Such broken lines are produced by fractional crystallization, mainly of plagioclase. REE patterns from the Khalkhab and Neshveh units can also be explained in terms of fractional crystallization. Using trace elements and Sr and Nd isotope ratios reveals that metasomatized mantle components have played a role in the genesis of the northwest Saveh intrusions. Based on tectonic discrimination diagrams, the rocks in this study were formed in an active continental margin during the convergence of the Arabia and Iran plates.

Acknowledgments

The authors would like to thank Shahrood and Tehran universities for supporting this project under grants provided by their research council. We are grateful to Fereshte Sajjdi and Afsaneh Dehbozorgi for microfossil recognition.

References

- Agard, P., Jolivet, L., Vrielynck, B., Burov, E., Monie, P., 2007. Plate acceleration: the obduction trigger? *Earth and Planetary Science Letters*, 258: 428-441.
- Agard, P., Monié, P., Gerber, W., Omrani, J., Molinaro, M., Labrousse, L., Vrielynck, B., Meyer, B., Jolivet, L., Yamato, P., 2006. Transient, syn-obduction exhumation of Zagros blueschists inferred from P–T–deformation–time and kinematic constraints: implications for Neotethyan wedge dynamics. *Journal of Geophysical Research* 111. doi: 10.1029/2005JB004103.
- Ahmadi Khalaji, A., Esmaily, D., Valizadeh, M.V., Rahimpour-Bonab, H., 2007. Petrology and geochemistry of the granitoid complex of Boroujerd, Sanandaj–Sirjan Zone, Western Iran. *Journal of Asian Earth Sciences*, 29: 859–877.
- Alavi, M., 1994. Tectonics of the Zagros orogenic belt of Iran: new data and interpretations. *Tectonophysics*, 229: 211–238.
- Amidi, S.M., 1984. Geological map of Saveh Quadrangle (scale 1:250000). Geological survey of Iran.
- Arvin, M., Pan, Y., Dargahi, S., Malekizadeh, A., Babaei, A., 2007. Petrochemistry of the Siah-Kuh granitoid stock southwest of Kerman, Iran: Implications for initiation of Neotethys subduction. *Journal of Asian Earth Sciences* 30: 474–489.
- Bea, F., Fershtater, G.B., Montero, P., Smirnov, V.N., Molina, J.F., 2005. Deformation-driven differentiation of granitic magma: The Stepninsk pluton of the Uralides, Russia. *Lithos*, 81: 209–233.
- Beard, J.S., Lofgren, G.E., Sinha, A.K., Tollo, R.P., 1994. Partial melting of apatite-bearing charnockite, granulite, and diorite: melt compositions, restite mineralogy, and petrologic implications. *Journal of Geophysical Research* 99: 21591–21603.
- Beard, J.S., Lofgren, G.E., 1991. Dehydration melting and water-saturated melting of basaltic and andesitic greenstones and amphibolites. *Journal of Petrology*, 32: 365–401.
- Berberian, F., Berberian, M., 1981. Tectono-plutonic episodes in Iran. In: *Zagros. Hindu Kush. Himalaya Geodynamic Evolution* Edited by H.K. Gupta, and F.M Delany, American Geophysical Union, Geodynamic Series Volume3, 1981.
- Berberian, F., Muir, I.D., Pankhurst, R.J., Berberian, M., 1982. Late Cretaceous and early Miocene Andean-type plutonic activity in northern Makran and Central Iran. *Geological Society of London*, 139: 605–614.
- Boudier, F., Ceuleneer, G., Nicolas, A., 1988. Shear zones, thrusts and related magmatism in the Oman ophiolite: initiation of thrusting on an oceanic ridge. *Tectonophysics*, 151: 275–296.
- Boynton, W.V., 1984. Cosmochemistry of the rare earth elements: Meteorite studies, in Henderson, P., (eds) *Rare earth element geochemistry*. Elsevier, Amsterdam, 63-114.
- Chappell, B.W. and White, A.J.R., 1974. Two contrasting granite types. *Pacific Geology*, 8: 173-174.
- Chappell, B.W., 1996. Magma mixing and the production of compositional variation within granite suites: evidence from the granites of southeastern Australia. *Journal of Petrology*, 37: 449-470.

- Chappell, B.W., 1999. Aluminium saturation in I- and S-type granites and the characterization of fractionated haplogranites. *Lithos*, 46: 535–51.
- Chappell, B.W., White, A.J.R., 1992. I- and S-type granites in the Lachlan Fold Belt. *Transactions to the Royal Society of Edinburgh: Earth Sciences*, 83: 1–26.
- Davarpanah, A., 2009. *Magmatic Evolution of Eocene. Volcanic Rocks of the Bijgerd-Kuh-e Kharchin area, Urumieh-Dokhtar Zone, Iran*. Master of Science thesis, Georgia State University. 138 pp.
- Davidson, J.P., 1996. Deciphering mantle and crustal signature in subduction zone magmatism. In: Bebout, G.E., Scholl, D.W., Kirby, S.H., Platt, J.P. (Eds.), *Subduction: Top to Bottom*. American Geophysical Union, Washington DC 251–262.
- DePaolo, D.J., 1981. Trace element and isotopic effects of combined wall rock assimilation and fractional crystallization. *Earth and Planetary Science Letters*, 53: 189–202.
- DePaolo, D.J., Linn, A.M., Schubert, G., 1991. The continental crustal age distribution; methods of determining mantle separation ages from Sm–Nd isotopic data and application to the Southwestern United States. *Journal of Geophysical Research* 96: 2071–2088.
- Dufek, J., Bergantz, G.W., 2005. Lower crustal magma genesis and preservation: a stochastic framework for the evaluation of basalt-crust interaction. *Journal of Petrology*, 46: 2167–2195.
- Fujinawa, A., 1992. Distinctive REE patterns for tholeiitic and calc-alkaline magma series co-occurring at Adatara volcano, Northeast Japan. *Geochemical Journal*, 26: 395–409.
- Ghalamghash, J., 1998. Geological map of Saveh Quadrangle (scale 1:100000). Geological survey of Iran.
- Ghasemi, A., Talbot, C.J., 2006. A new tectonic scenario for the Sanandaj-Sirjan Zone (Iran). *Journal of Asian Earth Science*, 26: 683–693.
- Greene, A.R., DeBari, S.M., Kelemen, P.B., Blusztajn, J., Clift, P.D., 2006. A detailed geochemical study of island arc crust: the Talkeetna arc section south-central Alaska. *Journal of Petrology*, 47: 1051–1093.
- Hoskin, P.W.O., 2000. Patterns of chaos: fractal statistics and the oscillatory chemistry of zircon. *Geochimica et Cosmochimica Acta*, 64: 1905–1923.
- Irvine, T.N., Baragar, W.R.A., 1971. A guide to the chemical classification of the common volcanic rocks. *Canadian Journal of Earth Sciences*, 8: 523–548.
- Jagoutz, O., Schmidt, M.W., 2012. The formation and bulk composition of modern juvenile continental crust: the Kohistan arc. *Chemical Geology*, 298–299: 79–96.
- Johnston, A.D., Wyllie, P.J., 1988. Constraints on the origin of Archean trondhjemites based on phase relations of Nùk gneiss with H₂O at 15 kbar. *Contributions to Mineralogy and Petrology*, 100: 35–46.
- Kohut, M., Nabelek, P.I., 2008. Geochemical and isotopic (Sr, Nd and O) constraints on sources of Variscan granites in the Western Carpathians—implications for crustal structure and tectonics. *Journal of Geosciences*, 53: 307–322.
- Kretz, R., 1983. Symbols for rock-forming minerals. *American Mineralogist*, 68: 277–279.
- Kuritani, T., Kitagawa, H., Nakamura, E., 2005. Assimilation and fractional crystallization controlled by transport process of crustal melt: implications from an alkali basalt dacite suite from Rishiri Volcano, Japan. *Journal of Petrology*, 46: 1421–1442.
- Lee, C.T.A., Bachmann, O., 2014. How important is the role of crystal ractionation in making intermediate magmas? Insights from Zr and P systematics. *Earth and Planetary Science Letters*, 393: 266–274.
- Macdonald, R., Hawkesworth, C.J., Heath, E., 2000. The Lesser Antilles volcanic chain: a study in arc magmatism. *Earth-Science Reviews*, 49: 1–76.
- Mc Culloch, M.T., Gamble, J.A., 1991. Geochemical and geodynamical constraints on subduction zone magmatism. *Earth and Planetary Science Letters*, 102: 358–374.
- McQuarrie, N., Stock, J.M., Verdel, C., Wernicke, B.P., 2003. Cenozoic evolution of Neotethys and implications for the causes of plate motions. *Geophysical Research Letters* 30: 2036, SED 6-1 to 6-4 doi: 10.1029/2003GL017992.
- Meyer, B., Mouthereau, F., Lacombe, O., Agard, P., 2005. Evidence for Quaternary activity along the Deshir Fault: Implication for the Tertiary tectonics of Central Iran. *Geophysical Journal International*, 163: 1–10.
- Mitropoulos, P., Saunders, A.D., Marsh N.G., 1987. Petrogenesis of Cenozoic volcanic rocks from the Aegean Island Arc. *Journal of Volcanology and Geothermal Research*, 32: 177–193.
- Mobasher, K., Babaie, H.A., 2008. Kinematic significance of fold- and fault-related fracture systems in the Zagros mountains, southern Iran. *Tectonophysics*, 451: 156–169.
- Molinaro, M., Guezou J.C., Leturmy, P., Eshraghi, S.A., Frizon de Lamotte, D., 2004. The origin of changes in structural style across the Bandar Abbas syntaxis SE Zagros (Iran). *Marine and Petroleum Geology*, 21: 735– 752.
- Molinaro, M., Zeyen, H., Laurencin, X., 2005. Lithospheric structure beneath the southeastern Zagros Mountains, Iran: recent slab break-off? *Terra Nova*, 17: 1–6.
- Nicolas, A., 1989. *Structures of ophiolites and dynamics of oceanic lithosphere*. Kluwer Dordrecht Publishing. 367 pp.

- Omran, J., Agard, P., Whitechurch, H., Benoit, M., Prouteau, G., Jolivet, L., 2008. Arc-magmatism and subduction history beneath the Zagros Mountains, Iran: A new report of adakites and geodynamic consequences. *Lithos*, 106: 380-398.
- Otamendi, J.E., Ducea, M.N., Bergantz, G.W., 2012. Geological, petrological and geo-chemical evidence for progressive construction of an arc crustal section, Sierra de Valle Fertil, Famatinian Arc, Argentina. *Journal of Petrology*, 53: 761-800.
- Pearce, J.A., 1982. Trace element characteristics of lavas from destructive plate boundaries. In: Thorpe, R.S. (eds) *Andesites. Orogenic andesites and related rocks*. Wiley, New York. 525-548 pp.
- Pearce, J.A., Bender, J.F., De Long, S.E., Kidd, W.S.F., Low, P.J., Guner, Y., Saroglu, F., Yilmaz, Y., Moorbath, S., Mitchell, J.G., 1990. Genesis of collision volcanism in Eastern Anatolia, Turkey. *Journal of Volcanology and Geothermal Research*, 44: 189-229.
- Pearce, J.A., Harris, N.W., Tindle, A.G., 1984. Trace element discrimination diagrams for the tectonic interpretation of granitic rocks. *Journal of Petrology*, 25: 956-983.
- Popov, V.S., Tevelev, A.A., Bogatov, V.I., 1999. The Stepninsk pluton in the south Urals: relationships of plutonic rocks coming from mantle and crustal sources. *Izv. Vuzov. Geologiya i Razvedka*, 5: 52-68.
- Rapp, R.P., Watson, E.B., 1995. Dehydration melting of metabasalt at 8-32 kbar: implications for continental growth and crust mantle recycling. *Journal of Petrology*, 36: 891-931.
- Rapp, R.P., Watson, E.B., Miller, C.F., 1991. Partial melting of amphibolite/eclogite and the origin of Archean trondhjemites and tonalites. *Precambrian Research*, 51: 1-25.
- Ratajeski, K., Sisson, T.W., Glazner, A.F., 2005. Experimental and geochemical evidence for derivation of the El Capitan Granite, California, by partial melting of hydrous gabbroic lower crust. *Contributions to Mineralogy and Petrology*, 149: 713-734.
- Rezaei-Kahkhaei, M., 2011. *Geochronology and Geochemistry of the NW Saveh intrusive plutons (Central Iran)*. University of Tehran, 134 pages.
- Rickwood, P.C., 1989. Boundary lines within petrologic diagrams which use oxides of major and minor elements. *Lithos*, 22: 247-263.
- Ricou, L.E., 1971. Le croissant ophiolitique péri-arabe, une ceinture de nappes mise en place au crétacé supérieur. *Revue de géographie physique et de géologie dynamique*, 13: 327-350.
- Ricou, L.E., 1994. Tethys reconstructed: plates, continental fragments and their boundaries since 260 Ma from Central America to South-eastern Asia. *Geodinamica Acta*, 7: 169-218.
- Rollinson, H.R., 1993. *Using Geochemical Data: Evaluation, Presentation, Interpretation*. Longman, Edinburgh Gate Publishing. 352 pp.
- Saunders, A.D., Tarney, J., 1979. The geochemistry of basalts from a back-arc spreading center in the East Scotia Sea. *Geochimica et Cosmochimica Acta*, 43: 555-72.
- Searle, M.P. and Cox, J., 1999. Tectonic setting, origin and obduction of the Oman ophiolite. *Geological Society of America Bulletin*, 111: 104-122.
- Shand, S.J., 1943. *Eruptive Rocks*. Murby Publishing, London, U.K. 360 pp.
- Spera, F.J., Bohron, W.A., 2001. Energy-constrained open system magmatic processes I: General model and energy-constrained assimilation and fractional crystallization (EC-AFC) formulation. *Journal of Petrology*, 42: 999-1018.
- Springer, W., Seck, H.A., 1997. Partial fusion of basic granulites at 5 to 15 kbar: implications for the origin of TTG magmas. *Contributions to Mineralogy and Petrology*, 127: 30-45.
- Steiger, R.H., Jaeger, E., 1977. Subcommission on geochronology: convention on the use of decay constants in geo- and cosmochronology. *Earth and Planetary Science Letters*, 36: 359-362.
- Sun, S.S., McDonough, W.F., 1989. Chemical and isotopic systematics of oceanic basalts: implications for mantle composition and processes. In: Saunders AD, Norry MJ (eds) *Magmatism in the Ocean Basins*. Geological Society of London, Special Publications, 42: 313-345.
- Talebian, M., Jackson, J., 2004. A reappraisal of earthquake local mechanisms and active shortening in the Zagros mountain of Iran. *Geophysical Journal International*, 156: 506-526.
- Tatsumi, Y., Eggins, S., 1995. *Subduction Zone Magmatism*. Blackwell Sciences Publishing, Oxford. 211pp.
- Tatsumi, Y., Suzuki, T., 2009. Tholeiitic vs Calc-alkalic Differentiation and Evolution of Arc Crust: Constraints from Melting Experiments on a Basalt from the Izu-Bonin-Mariana Arc. *Journal of Petrology*, 50: 1575-1603.
- Taylor, S. R., McLennan, S. M., 1985. *The Continental Crust: Its Composition and Evolution*. Blackwell, Oxford, p. 1-312.
- Thompson, A.B., Matile, L., Ulmer, P., 2002. Some thermal constraints on crustal assimilation during fractionation of hydrous, mantle derived magmas with examples from central Alpine batholiths. *Journal of Petrology*, 43: 403-422.
- Tupinambá, M., Heilbron, M., Valeriano, C., Porto Júnior, R., de Dios, F.B., Machado, N., Silva, L.G.E., Almeida, J.C.H., 2012. Juvenile contribution of the Neoproterozoic Rio Negro Magmatic Arc (Ribeira Belt, Brazil): Implications

- for Western Gondwana amalgamation. *Gondwana Research*, 21: 422-438.
- Vernant, P., Nilforoushan, F., Hatzfeld, D., Abbassi, M.R., Vigny, C., Masson, F., Nankali, H., Martinod, J., Ashtiani, A., Bayer, R., Tavakoli, F., Chery, J., 2004. Present-day crustal deformation and plate kinematics in the Middle East constrained by GPS measurements in Iran and northern Oman. *Geophysical Journal International* 157: 381–398.
- White, A.J.R., Chappell, B.W., 1983. Granitoid types and their distribution in the Lachlan Fold Belt, southeastern Australia. *Geological Society of America Memoir* 159: 21-34.
- Wilson, M., 2007. *Igneous Petrogenesis*. Chapman & Hall, London, 411p.
- Winter, J.D., 2001. *An Introduction to Igneous and Metamorphic Petrology*. New Jersey: Prentice Hall. 699 p.
- Winther, K.T., 1996. An experimentally based model for the origin of tonalitic and trondhjemitic melts. *Chemical Geology*, 127: 43–59.
- Wolf, M.B., Wyllie, P.J., 1994. Dehydration-melting of amphibolite at 10 kbar: The effects of temperature and time. *Contributions to Mineralogy and Petrology*, 115: 369-83.
- Workman, R.K., Hart, S.R., 2005. Major and trace element composition of the depleted MORB mantle (DMM). *Earth and Planetary Science Letters*, 231: 53-72.
- Wyborn, D., Chappell, B.W., James, M., 2001. Examples of convective fractionation in high temperature granites from the Lachlan Fold Belt. *Australian Journal of Earth Sciences*, 48: 531–541.